LHCf

Technical Proposal for the LHC Run3

Addressing Cosmic Ray physics with forward measurements in proton–proton and proton–light nuclei collisions at LHC

CERN-LHCC-2019-008 / LHCC-P-014
20/06/2019

List of authors

O. Adriani[1,2], E. Berti[1,2], L. Bonechi[1], M. Bongi[1], R. D'Alessandro[1,2], M. Haguenauer[4], Y. Itow[5,6], K. Kasahara[7], Y. Matsubara[5], H. Menjo[5], Y. Muraki[5], K. Ohashi[5], P. Papini[1], S.B. Ricciarini[1,3], T. Sako[8], N. Sakurai[9], K. Sato[5], Y. Shimizu[10], T. Tamura[10], A. Tiberio[1,2], S. Torii[7], A. Tricomi[11,12], M. Ueno[5], and K. Yoshida[13]

[1]INFN Firenze, Italy
[2]University of Florence, Italy
[3]IFAC-CNR and INFN Firenze, Italy
[4]École-Polytechnique, Paris, France
[5]ISEE, Nagoya University, Nagoya, Japan
[6]KMI, Nagoya, Japan
[7]RISE, Waseda University, Tokyo, Japan
[8]ICRR, University of Tokyo, Kashiwa, Chiba, Japan
[9]Tokushima University, Tokushima, Japan
[10]Kanagawa University, Yokohama, Japan
[11]INFN Catania, Italy
[12]University of Catania, Italy
[13]Shibaura Institute of Technology, Saitama, Japan

June 14, 2019

Abstract

The LHCf experiment was originally designed to measure neutral particles produced at very high pseudo-rapidity ($\eta > 8.4$) in $p + p$ collisions at an energy of 14 TeV in the center of mass frame and in p+A collision. Since the first activities at the LHC in 2009, the LHCf detectors have taken data in different conditions involving proton and ions with different energies. The measurements carried out so far concern $p + p$ collisions at $\sqrt{s}$=0.9, 2.76, 7 and 13 TeV and $p + Pb$ collisions at $\sqrt{s_{NN}}$=5 TeV and 8 TeV. These cases correspond to proton collisions in the laboratory frame with an equivalent energy ranging from 10^{14} eV to almost 10^{17} eV, thus covering a large energy range which is significant for the study of the highest energy cosmic-rays interactions with the atmosphere. These data are extremely useful for the calibration of hadronic interaction models used for the study of the development of atmospheric showers, the so called Extensive Air Showers (EAS), produced by extremely energetic cosmic-ray (CR) particles interacting with the atmospheric gas. Because of the characteristics of these collisions, the study of the $p + p$ system only at LHC is not enough to have a complete picture of the real processes going on in the Earth atmosphere, where interactions involve mainly nitrogen and oxygen nuclei. The dynamic of $p + N$ collisions can differ in many important aspects with respect to the more simple case of $p+p$ interactions. For example, a significant reduction in the cross section in $p+A$ with respect to $p+p$ collisions, due to nuclear screening effects, has been found in previous measurements performed at smaller values of pseudo-rapidity and lower energy than the LHC; this reduction has been later confirmed by LHCf itself by comparing $p + p$ with $p + Pb$ interactions.

In this document we propose to install the LHCf detectors for the $p+p$ run at $\sqrt{s}$=14 TeV and for the eventual proton - light ion run that is under discussion after the first year of the LHC Run3. The main purpose of this proposal is to get a better understanding of the nuclear effects in a pseudo-rapidity and energy configuration that is very significant for CR physics, with the aim to reduce the systematic uncertainties still present in the High Energy hadronic interaction models. As an additional by-product, we can extend at 14 TeV the measurements already carried out by LHCf at smaller center of mass energies; thanks to the improved DAQ system, which allows more than the double of the previous DAQ rate, and to a more sophisticated trigger scheme, allowing to operate at a luminosity 10 times higher than before, we can significantly increase the statistics of our measurements. This will give us the opportunity to measure also the spectra of neutral hadrons others than π^0 very forward produced in the $p + p$ and p+Light Ion collisions.

Contents

List of Figures

List of Tables

1 Introduction

The knowledge of the hadronic interaction models is a key ingredient for a proper description of the properties of Ultra High Energy Cosmic Rays (UHECR). Indeed, despite the significant improvement in our understanding of UHECR properties thanks to the excellent performance of the giant hybrid arrays, like the Auger and TA experiments, still the results are largely affected by the poor knowledge of the nuclear interaction mechanism of primary cosmic rays with the Earth's atmosphere. In the analyses of observed data, comparison with Monte Carlo simulations of air showers is unavoidable, and the results are sensitive to the choice of the hadronic interaction model used in the simulation [2]. Data collected at LHC provides a very important opportunity to calibrate the Monte Carlo codes used. Thanks to the LHC Run1 data, some interaction models have been updated, and the dispersion found in the predictions of air shower observables decreased. However, there is still significant difference between the model predictions and the data especially in the forward region where particle production is particularly important since they carry a large fraction of the total collision energy and are responsible to determine the shape of air showers [3].

The Large Hadron Collider forward (LHCf) experiment was designed with the aim to provide a calibration of the hadronic interaction models in the whole energy range spanned by LHC by measuring the neutral forward particle produced in $p + p$ as well as in p+Ion collisions, accessing the rapidity range from 8.4 to infinity. The major objectives of the LHCf project are to determine the differential production cross sections of photons, neutrons and neutral pions thus providing new information about high-energy hadronic interactions, due to its unique phase space coverage. LHCf is the only experiment in the world that performs this type of high-precision study in measuring energy and pseudo-rapidity of the single detected particles.

Physics results from LHCf constitute a firm basis for the calibration of hadronic interaction models that are commonly used for the simulation of the development of cosmic-ray showers developing in the Earth atmosphere. Atmospheric cosmic-ray showers, or extensive air showers (EAS), are huge cascades of secondary particles produced by the interaction with the atmospheric gas of primary cosmic rays, elementary particles coming from the outer space with energies that can reach extreme values, around 10^{20} eV.

The energy flow in the showers is dominated by particles and nuclear fragments that are emitted at very small angles with respect to the arrival direction of the incoming projectile. For this reason LHCf is designed in such a way to cover the pseudo-rapidity region from 8.4 up to infinity (the so called very forward region).

Since 2009 the LHCf experiment has collected data at different collision energies and with different colliding particles. Most operations were carried out under dedicated conditions, i.e. configured as special runs at low luminosity to avoid pileup and high β^* to reduce the angular spread due to the beam divergence at the interaction point. Since 2015, the LHCf and ATLAS experiments have exchanged trigger information to allow

a common data taking, with the aim perform common analyses exploiting central and forward measurements at the same time. In Table 1 a summary of the LHCf operations and analyses are reported.

Year	Energy [TeV]	Collisions	Detector	Papers		
				γ	n	π^0
2009-2010	0.9	p-p	ARM1 & ARM2	[4]		
2010	7	p-p	ARM1 & ARM2	[5]	[6]	[1, 7]
2013	2.76	p-p	ARM1 & ARM2			[1, 8]
2013	5.02	p-Pb	ARM2			[1, 8]
2015	13	p-p	ARM1 & ARM2	[9, 10]	[11]	
2016	5.02	p-Pb	ARM2			
2016	8.16	p-Pb	ARM2			

Table 1: Summary of the LHCf runs at LHC and analysis matrix.

The pre-LHC hadron interaction models show large discrepancies in predictions with respect to the LHC results, however they have been significantly improved by using both central and forward measurements performed at LHC. While the general features of QCD, like quark confinement, multiple interactions and jet production, are included in all the models, particular features that are relevant for the development of air showers, like diffraction dissociation and forward particle flow are still not fully satisfactorily described. This is reflected in the fact that the agreement between the LHC data and MC model predictions are generally good in the central region while are still poor in the forward region. Even in the most recent versions of the MC models, the description of the leading particle behaviour is not yet in agreement with data. The only available data for such tuning are indeed those provided by the LHCf experiment. Lack of data, or even low statistics in the leading meson production in the very forward region, is one of the main reasons why this discrepancy has not yet been fixed. In fact, while the models after LHC Run2 reproduce better the spectral shape in the Feynman variable, x_F, the transverse momentum distribution is not yet well described. One of the central assumptions in the analytic calculations of the atmospheric fluxes is the scaling behavior (energy independence) of the particle production spectra at large Feynman-x, the so-called Feynman scaling. According to LHCf previous measurements the scaling hypothesis holds within a $\simeq 10\%$ precision. In the calculation of the atmospheric fluxes the production spectra in the very forward region play a crucial role. The increase of statistics as well the possibility to take data at the highest available energy would certainly help to further reduce the discrepancy between data and MC prediction as well as to provide further input to study the validity of the Feynman scaling.

The Physics motivation for taking data with the LHCf detector at LHC-Run3 are discussed in detail in section . 2, while in sections 3 and 4 the achievable goals in a future p-p run at $\sqrt{s} = 14$ TeV and with $p + O$ collisions at $\sqrt{s_{NN}} = 9.9$ TeV,

respectively, are addressed. Details of the needed detector upgrade and of the re-installation procedure are discussed in section 5. Requirements to take data during the $p + p$ run as well in a possible $p + O$ or $O + O$ run are finally discussed in section 6. In addition, in section 3.2 future improvements coming from a combined data analysis with the ATLAS forward detectors are discussed.

1.1 The LHCf detectors

The LHCf experimental apparatus is composed of two independent detectors, called Arm1 and Arm2, that can measure forward particles at 140 m from the ATLAS interaction point. The installation position is inside the so called recombination chamber, the region where the beam pipe makes a transition from a single big-diameter pipe to two small-diameter pipes which are connected to the LHC arc. The LHCf detectors can be inserted into an instrumentation slot obtained inside the massive TAN absorbers, a 10 cm large cavity that allows accessing the space between the two small-diameter pipes, i.e. the region up to zero degree with respect to the beam interaction line. At runtime, the LHCf detectors are installed in the nearest positions facing IP1, Arm1 in the LSS1L zone (IP8 side) and Arm2 in the LSS1R zone (IP2 side), i.e. just upstream of the BRAN and the ATLAS ZDC detectors. In this position the LHCf detectors can access the interaction line looking towards IP1 with no material along their line of sight, except for the wall of the beam pipe that has a projected thickness of approximately one radiation length. They can therefore measure very precisely particles emitted at zero degree or at very small angles. Because of the presence of the D1 dipole magnets between IP1 and the detectors, the LHCf only neutral particles can arrive at the LHCf location, like photons and neutrons.

Each one of the LHCf detectors (see figure 1) contains two independent sampling and imaging calorimeter towers with square section, which are made of tungsten plates, GSO scintillator layers for the longitudinal shower sampling and tracking layers for measuring the center of detected showers and their transverse profiles, thus allowing also to identify events with multiple incident particles. While the calorimetric systems are identical for the two detectors, the tracking systems are different: 4 X and 4 Y layers made of 1 mm square GSO fibers in Arm1 and microstrip silicon sensors in Arm2. The transverse sizes of the towers are of few centimeters, 2 cm × 2 cm and 4 cm × 4 cm for Arm1 and 2.5 cm × 2.5 cm and 3.2 cm × 3.2 cm for Arm2. The "two-towers" configuration is designed to maximize the detector performance for the study of events with two detected particles, like the two gamma rays from neutral pion decay.

In the default running configuration, the detectors are positioned with the two smaller calorimeters intercepting the interaction line, thus covering the pseudorapidity region up to extreme values (zero degree). The maximum pseudorapidity coverage of the detectors is approximately η >8.4 and is reached when running with a full beam crossing angle around 290 μrad. The energy resolution is better than 5% for photons and about (35÷40)% for neutrons. The position resolutions for photons and neutrons

Figure 1: LHCf (left) Arm1 and (right) Arm2 detectors.

are better than 0.2 mm and 1 mm, respectively.

2 Physics motivation: opportunities for LHCf in the LHC Run3

A detailed description of the interaction of CRs in the Earth's atmosphere requires the precise knowledge of the high energy interactions between the protons and the nuclei of the molecules constituting the atmosphere; the starting point for the generation of the Extended Air Showers (EAS) in the atmosphere is in fact the hadronic interaction of a single highly energetic primary cosmic ray with a nucleus of the atmosphere, mainly nitrogen and oxygen, and the details of this primary interaction (like for example the cross section, the inelasticity and the spectra of the produced secondary particles) are important for a precise description of the development of the EAS. Another important point is related to the fact that the composition of the very high energy cosmic rays is still not clear: they can be protons, but they can also be light or heavy nuclei [12]. The study of forward physics in p+p and p+A collisions at high energy at LHC is important for a detailed understanding of the properties of the HECR hadronic interactions in the atmosphere, since the energy available in the center of mass system at LHC ($\simeq$ 14 TeV), properly boosted with the Lorentz transformation, correspond to an energy of $\simeq 10^{17}$ eV in the laboratory frame. Additionally, the forward region is important since most of the energy of the debris of the hadronic interactions is concentrated in

this region.

The opportunity for LHCf to take data during the LHC Run3 period is therefore important to shade additional light on the physics of the hadronic interaction of CRs with the atmosphere, and to additionally contribute to an improvement of the hadronic interaction models.

The main physics motivation for this proposal are the following:

- $p + p$ collisions at 14 TeV.

  The opportunity to take data in the Run3 $p + p$ collisions at 14 TeV will allow LHCf to additionally extend the range of center of mass energies explored during the previous $p + p$ runs [4, 5, 6, 9, 11, 1]. We do not expect a significant change with respect to the latest basic results obtained with the 2015 $p+p$ run at 13 TeV on the comparison between several hadronic interaction models used in Cosmic-ray physics, due to the limited increase of the energy. However, we expect to improve in a significant way the physics outcome of our results, thanks to the on-going hardware upgrade, to a new trigger strategy and to the possible data taking jointly carried out with the Atlas forward detectors. The hardware upgrade and a new trigger scheme allow us to operate at 10 times higher luminosity than in the 2015 13 TeV $p + p$ run. Consequently we can improve the statistics of events for which LHCf has a small acceptance, thus opening the possibility to measure spectra of neutral mesons different from the π^0, like η and K^0. THe LHCf collaboration is proposing also to prepare a joint run with the ATLAS apparatus and the ATLAS collaboration has already confirmed their interest and support for a common data taking during $p + p$ collisions. The combined data taking with the ATLAS central and forward detectors would open the possibility to improve the diffractive and not-diffractive physics results.

- $p + O$ collisions

  The opportunity to take data in the Run3 collision between protons and light ions represents a real breakthrough for the HECR physics case. There is currently a serious interest in this type of collisions, not only for the HECR field, but also in other communities [13]. The most probable light ion collisions that are foreseen at LHC will use oxygen, that is among the best possible targets for the HECR physics case. As reported at the beginning of this section, the possibility to directly probe the high energy collisions happening in the atmosphere will allow a significant reduction of the systematic effects that are present in the extrapolation of the LHC directly measured quantities to the widely used high energy hadronic interaction models. This task can be accomplished through the direct measurement of the nuclear modification factor in $p + O$ collisions.

These two main physics cases will be highlighted in detail in the next sections.

3 Physics program with $p+p$ collisions at $\sqrt{s} = 14$ TeV

In this section the experimental results obtained so far are introduced and the most relevant expectations based on preliminary simulations of $p+p$ collisions at $\sqrt{s}$ =14 TeV are reported. The basic results obtained with the 2015 $p+p$ run at 13 TeV on the comparison between several hadronic interaction models used in Cosmic-ray physics are expected to change only slightly. Nevertheless, thanks to the higher energy, to the on-going detector upgrade, to a development of a new trigger strategy and to a possible common data taking with the ATLAS forward detectors, we expect to improve significantly the performance achievable in some analysis and to open new physics channels, thus defining a different purpose with respect to the previous runs and increasing the impact of the LHCf program on the astroparticle and high energy physics communities.

3.1 LHCf stand-alone physics program

3.1.1 Basic goals: photon, neutron and neutral pion spectra

The basic LHCf physics program for Run 3 includes the measurements of all the neutral components generated in the interactions which are dominant from a statistic point of view within the LHCf acceptance. It means basically three classes of events: single photons, single neutrons and single neutral pions, the last seen in the LHCf detectors as two independent photons hitting the two calorimeter towers separately in the easiest case (type I π^0 events). For these three types of events the global acceptance of one of the LHCf detector, is approximately 11.6% (6% single photons, 5.5% single neutrons and 0.1% neutral pions).

Top panel of figure 2 shows the photon energy spectra measured for $p+p$ collisions at 13 TeV (2015) in two different intervals of pseudorapidity, compared with simulations based on different hadronic interaction models [9]. The ratios of models to data are also shown. None of the models can reproduce satisfactorily the experimental points, but measurements are confined within models. The lower panel of the same figure shows the neutron spectra measured during the same run in three different intervals of pseudo-rapidity, compared with models [11]. In this case the description of the experimental data is even worse, especially at extreme pseudorapidity, where only the QGSJET II-04 model seems to reproduce approximately the experimentally observed high energy peak.

Simulations of $p+p$ collisions at 7 TeV proton energy at the LHC have been implemented to derive the relevant expectations for an eventual LHCf data taking in Run 3.

Two hadronic interaction models have been used, QGSJET II-04 [14] and DPMJET 3.06 [15], for which 2×10^6 and 8×10^6 collision have been generated respectively. Top left (right) plot of figure 3 shows the expected energy spectra of single photon events

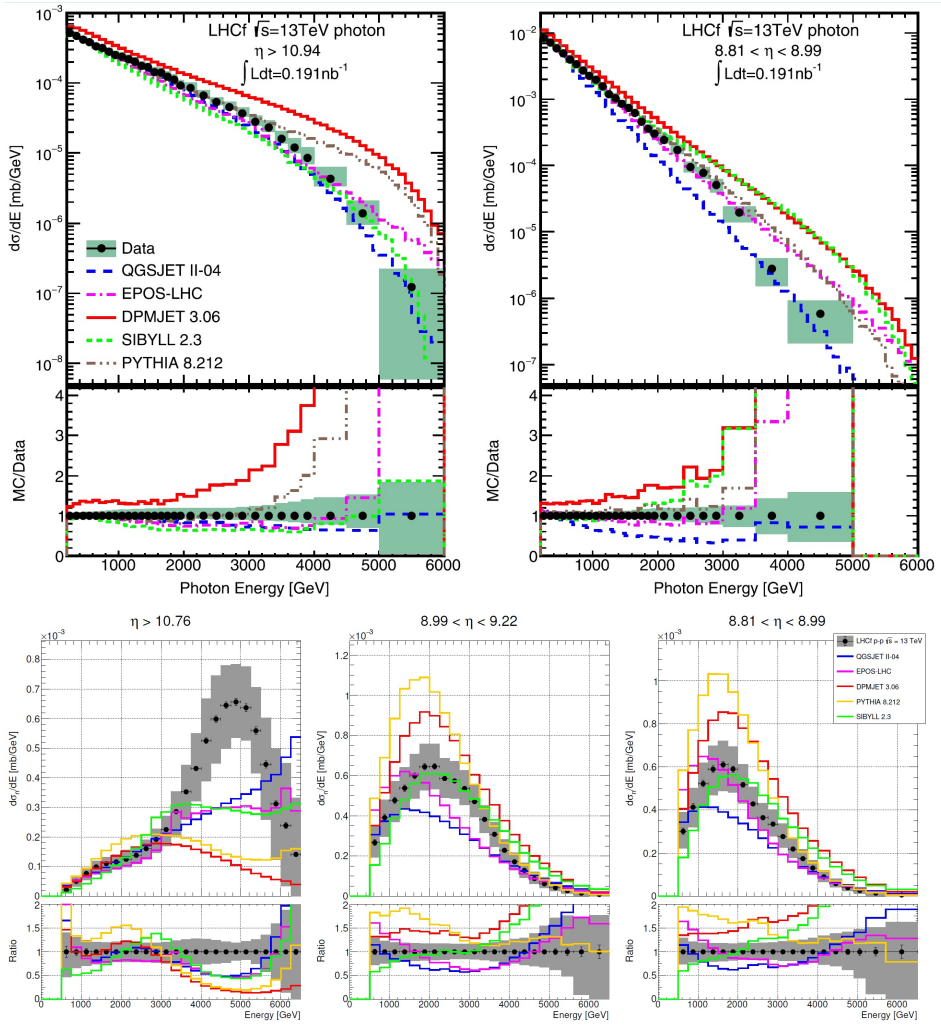

Figure 2: Photon (top panel) and neutron (bottom panel) spectra measured by the LHCf experiment in $p+p$ collisions at $\sqrt{s} = 13\,\text{TeV}$.

hitting the Arm2 small (large) calorimeter tower, predicted using the two models. Despite the important steps forward allowed by the LHC in providing measurements of cross sections at high energy, used for the calibration and fine tuning of the Monte Carlo codes, clear discrepancies are still found between the different models. The left (right) plot at the center shows the energy distribution of single neutrons entering the small (large) tower.

The two plots below shown the same neutron spectra after introducing a smearing obtained applying a 35% hadron energy resolution, which is characteristic of the LHCf calorimeters. The neutron spectrum has an important discrepancy between the models and further accurate measurements would be very appreciated by the cosmic-ray community. Unfortunately the depth of the sole LHCf detector is not appropriate for a precise determination of the hadron energy and an energy resolution better than 35% could not be achieved.

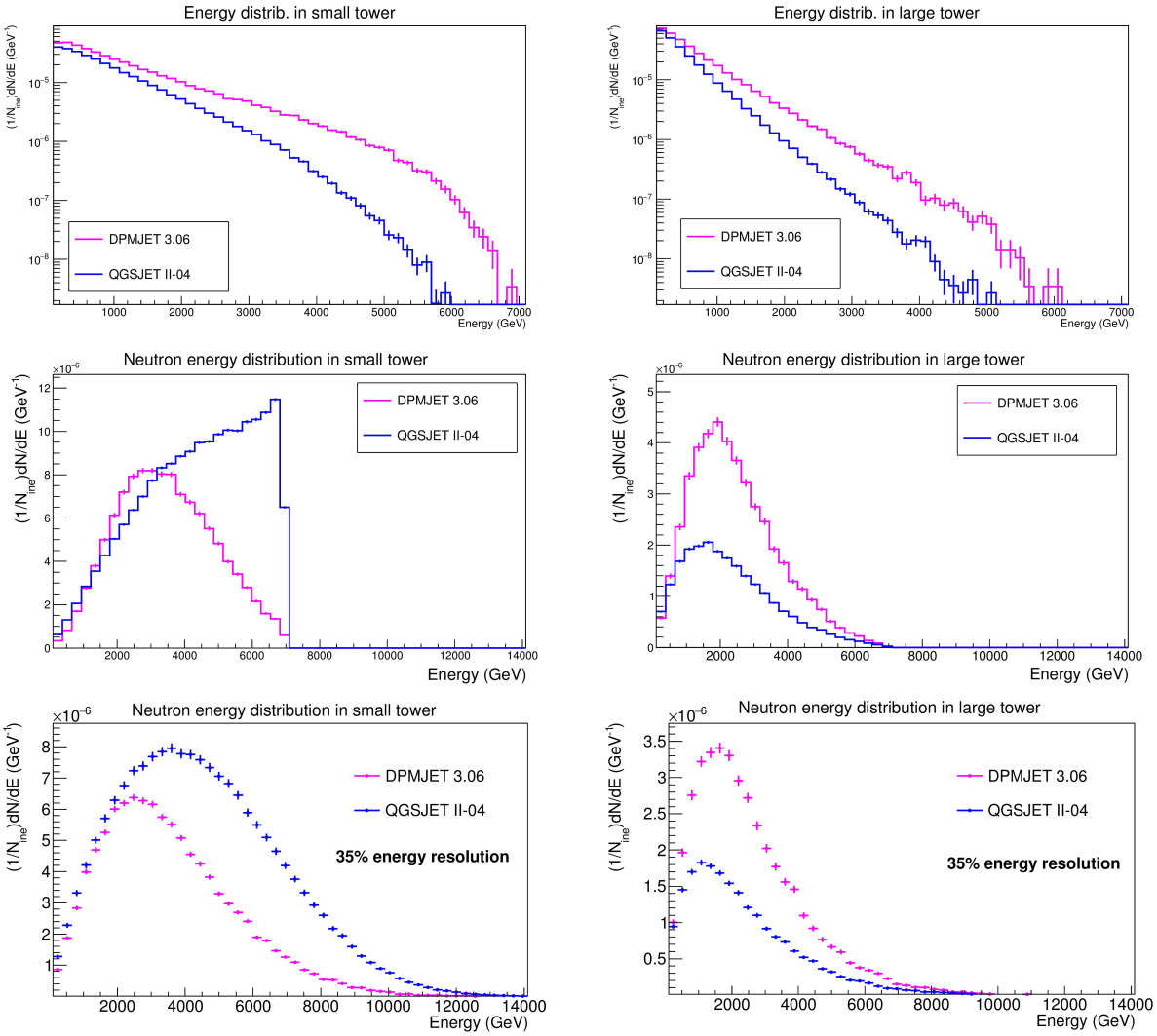

Figure 3: Top: energy distribution of photons detected in the Arm2 small (left plot) and large (right plot) calorimeter tower. Center: energy distribution of single neutrons detected in the small (left plot) and large (right plot) without taking into account any hadron energy resolution. Bottom: energy distribution of single neutrons after applying a 35% hadron energy resolution for the LHCf calorimeters.

The left plot of figure 4 shows the expected invariant mass distribution of gamma ray pairs with the two gamma rays hitting separately the two calorimeter towers (type I). Two peaks can be easily identified, corresponding to the masses of the neutral pion and eta meson. Approximately 10 thousands type 1 neutral pions can be selected with a background of the order of approximately 15%. The right plot of figure 4 shows the energy distribution of the selected pion sample predicted by the two models.

Figure 5 shows the ratio of the type 1 neutral pion spectra predicted by the two models. The discrepancy is confined within a factor 2 below 3.5 TeV and seems to slightly increase at higher energies.

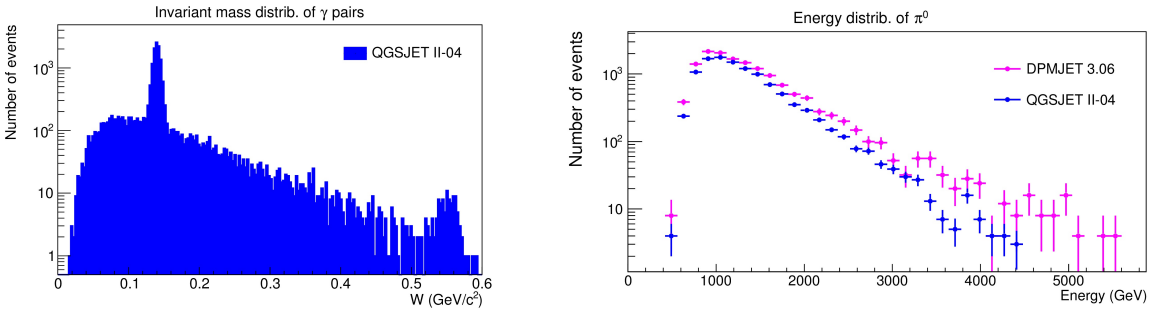

Figure 4: Left: reconstructed invariant mass distribution for events with photon pairs entering the two calorimeter towers separately. Right: Energy distribution of the type I neutral pion events expected in the LHCf Arm2 detector.

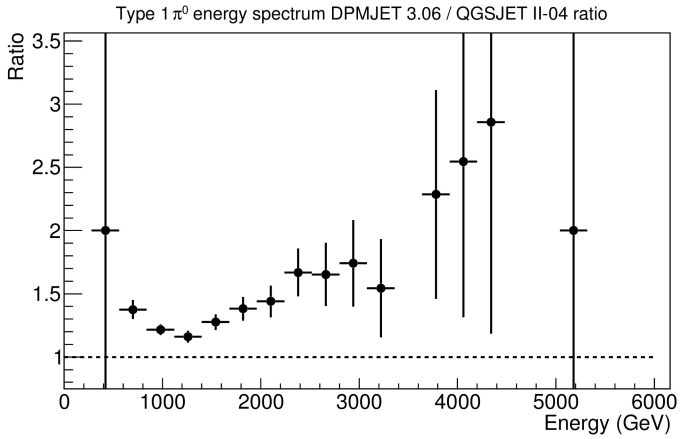

Figure 5: Ratio of the type I neutral pion energy spectra predicted by the two models used for the simulation of the $p + p$ collisions.

Due to the limited acceptance for neutral pions with respect to single photons or neutrons, a larger number of collisions is required in such a way to allow measuring the energy spectra in different intervals of the phase space, thus improving the information for model developers.

To enlarge the global acceptance of pions and extend the accessible phase space, type II events, defined as those events where the pair of gamma rays following the pion decay enter the same tower of the LHCf calorimeter, will be considered. These events are slightly more complicated to be studied from the experimental point of view at least for three main reasons. The first one is that the longitudinal shower development measured in the same tower is the sum of two gamma ray showers and is not therefore directly related to the energy of a single photon. The second one is that if the two gamma ray hits have a small spatial separation it is not trivial to separate their energy contributions. The third one is that if the two gamma rays have very different energies, the contribution of that with lower energy can be estimated with low precision due to the fluctuations on the energy releases of the other one.

Despite of these limitations the excellent performance of the LHCf detectors in terms of spatial resolution allows identifying and studying this type of events (see for example [1]). The identification of the impact points takes advantage of the good spatial resolution of the tracking detectors (0.2 mm for the Arm1 scintillating bars and better than 0.1 mm for the Arm2 microstrip silicon sensors).

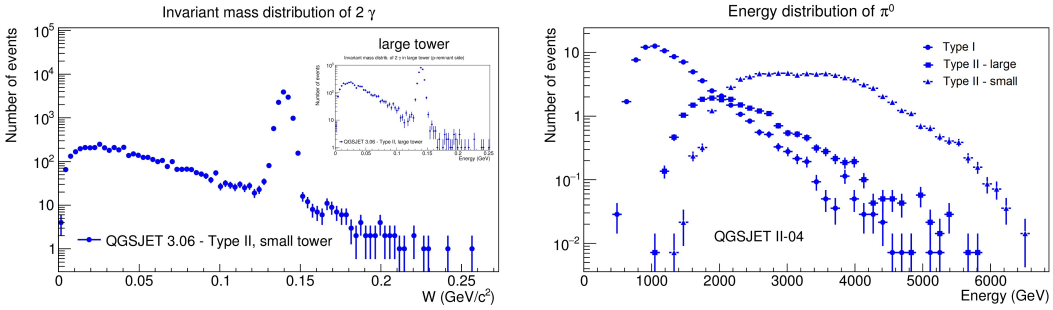

Figure 6: Left side: Invariant mass for the type II π^0 events in the small tower. Right side: Comparison between the energy distributions of Type I and Type II π^0 events, both in small and large towers.

The invariant mass distrbutions for this type of two-photon events expected in the small and large calorimeter towers are shown in the left plot of figure 6. In the right plot the energy distributions of the selected type I and type II π^0 events are compared. The number of expected type II π^0s in the small calorimeter tower is of the same order than the type I events, while for the large tower it is a factor 3 lower. The different region covered in the phase space can be more easily visualized in the p_t−x_F plane, where p_t is the transverse momentum and x_F the Feynman-x variable), as shown in figure 7. The left plot shows the type I event distribution. In the right plot the type II

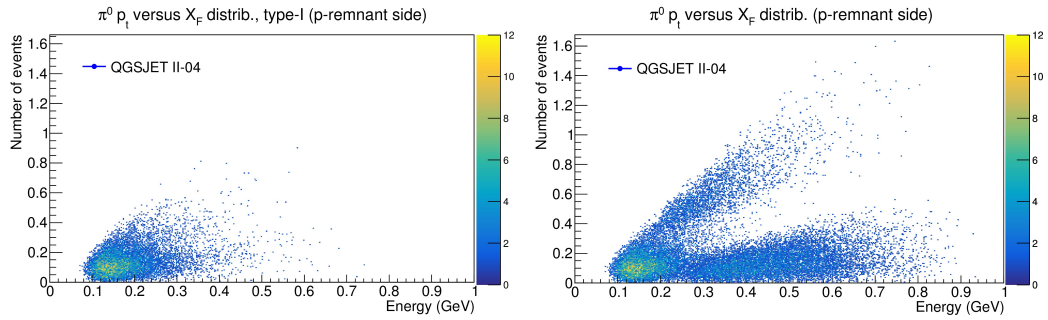

Figure 7: Left: expected distribution of type I π^0 events in the p_t−x_F plane. Right: expected distribution of type I + type II π^0 events in the p_t−x_F plane.

events are also included. Figure 8 shows the experimental distribution of events which have been detected in $p+p$ collisions at $\sqrt{s} = 13\,\text{TeV}$ in 2015.

The main purpose of the LHCf stand-alone program concerning the neutral pion component is the increase of the statistics previously accumulated at slightly lower

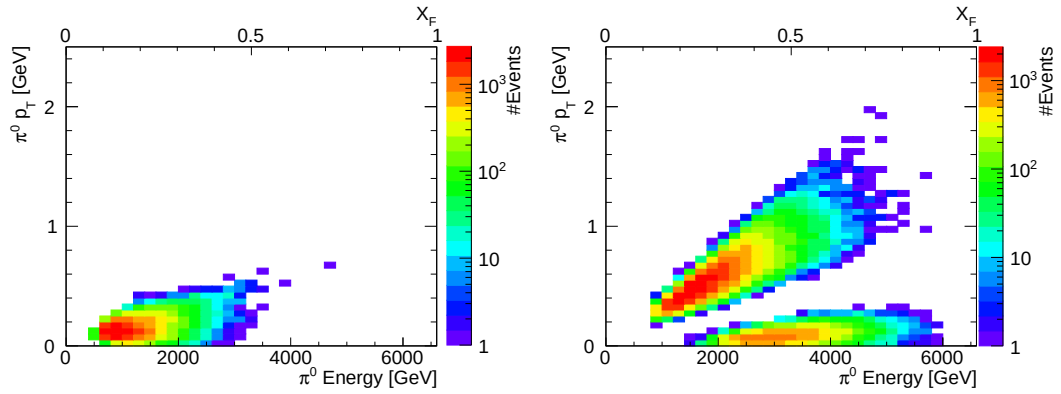

Figure 8: The distribution of π^0's collected by LHCf-Arm1 in the 2015 operation at $p+p$, $\sqrt{s}$= 13 TeV as functions of π^0 energy and p_{T}.

energy, that will be possible thanks to the upgrade of the Arm2 readout system, to a different trigger strategy that privileges the high energy showers and to the running at a nominal luminosity higher than the previous $p+p$ run. The expected statistical error of π^0 p_T spectrum in each X_{F} bin are shown in Figure 9.

The new measurements will allow reducing sensibly the statistical error bars and covering relevant regions of p_T in the high X_F region, that were not covered with data collected in the 13 TeV $p+p$ run.

3.1.2 Special program: LHCf rare events (η and K^0 mesons)

The contribution of the strange quark to the hadronization processes can be probed by measuring the production cross-sections of the η and K^0 mesons. The strange quark contribution is one of the parameters characterizing the different hadronic interaction models. A difference in this parameter induces a large discrepancy on the expected η production cross section among the models, an effect which is larger with respect to that related to π^0s, as shown in figure 10. Photons can be produced in several decay modes of η. These photons are the second dominant source of photon production in high energy hadronic interactions and contribute to the development of air showers induced by cosmic-rays. The measurement of the forward Kaon production is also important, for example in neutrino astronomy. Most of atmospheric muon neutrino in the TeV-PeV energy range are produced from charged kaon decays that take place in CR air showers and these are an important source of background for the astronomical neutrino search.

η measurement

η mesons decay mainly to photon pairs, following the $\eta \to 2\gamma$ decay channel with a branching ratio of 39.4%. These decays can be seen inside the LHCf detectors as two photons hitting the two calorimeter towers separately. The detection and event reconstruction methods for η are compatible with those of Type 1 π^0. A clear peak corresponding to the η mass can be easily identified in figure 4. The lower energy

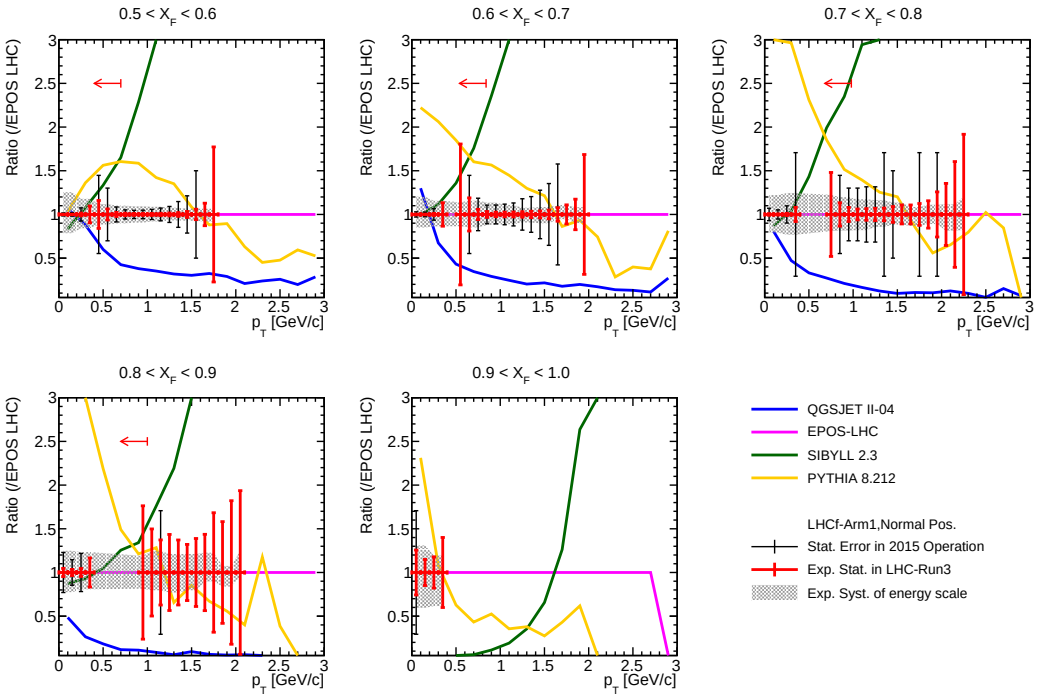

Figure 9: Expected statistical error sizes of π^0 p_T spectrum, relative to the EPOSLHC model, in different $X_{\rm F}$ bins. The black and red colored error bars represent the sizes of the statistical errors of data obtained by the Arm1 detector in 2015 and expectation in the LHC Run 3 operation. The expected systematic error due to the $\pm$3% energy scale error, which is a dominant source in these high $X_{\rm F}$ regions, is about 20-40% shown as gray hatched area. The spectra predicted by different models, normalized by the EPOS-LHC model, are shown by colored lines to give an idea of the model discrimination/calibration capability achievable with the LHCf measurements. The red small arrows on the top indicate the p_T coverage of the results at $p+p$, $\sqrt{s} = 7$ TeV [1]

.

threshold for η detection, E_{min} is about 2 TeV, as shown in the left plot of figure 11, which is much higher than for π^0's. This is related to the fact that the mass of the η meson is about a factor 4 higher than the mass of the π^0, since $E_{min} = 2\, m_{\pi^0\,(\eta)}\, L/d_{max}$, where $m_{\pi^0\,(\eta)}$ is the mass of the π^0 (η), L is the distance between IP1 and the LHCf detector, 140 m, and d_{max} is the maximum distance between the two photon hit positions in the detector acceptance, about 5 cm.

In the Arm1 data set taken in 2015 with $p+p$ collisions at $\sqrt{s} = 13$ TeV, corresponding to an integrated luminosity of 2 nb^{-1}, only about 500 η candidate events have been found. To nicely measure the differential cross-section of η production and to compare it with the model predictions, we require a higher statistics, at least a factor 10 more than that already accumulated.

K^0 measurement

The challenging measurement of forward K^0s requires to simultaneously detect the

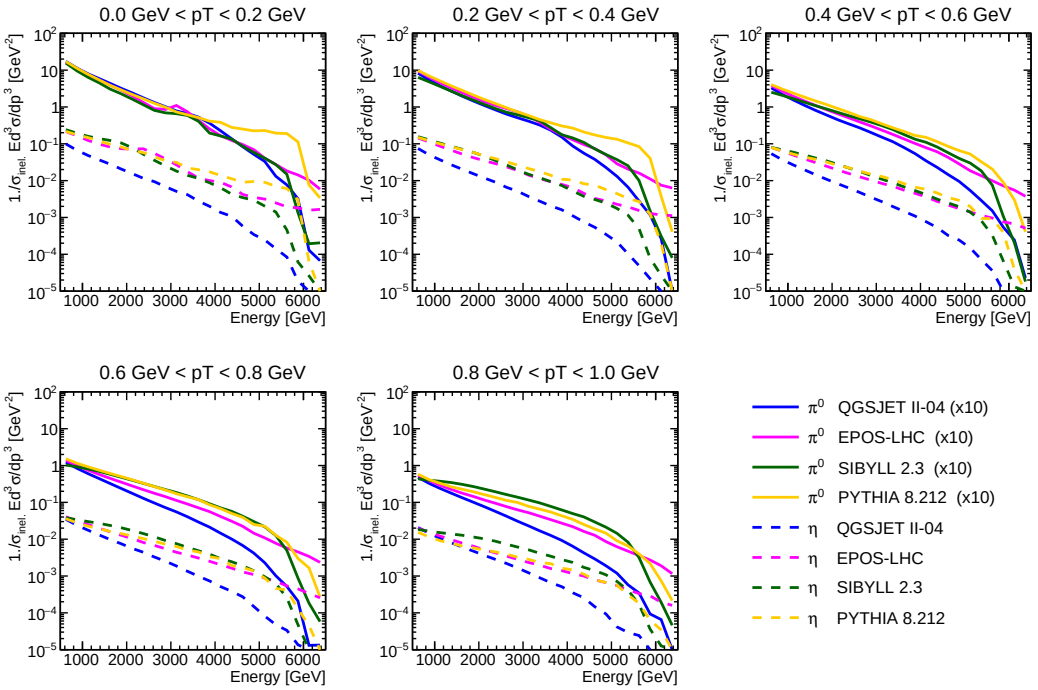

Figure 10: Model predictions for the production differential cross-section for π^0's and η's at $p+p$, $\sqrt{s}$= 13 TeV. The cross-sections of π^0's are scaled by a factor 10.

four photons from a K^0 decay; $K^0_s \to 2\pi^0 \to 4\gamma$ (BR: 30.7%). TeV-energy K^0s can fly inside the beam pipe from the interaction point and some of them decay before arriving at TAN. The K^0 decay vertex position can be estimated with the assumption that the invariant masses of photon pairs are equal to the π^0 mass. The kinematics of the K^0, in particular its energy, p_T, and mass as well as the decay vertex position, can be reconstructed from the measured energies and hit positions of the four photons. Because of the small probability of four photon detection in the LHCf detector, the geometrical acceptance for K^0 detection is very small, as shown in the right plot of figure 11. In 20 nb^{-1} data set, a few hundreds of K^0 candidate events can be collected, with an estimated background of approximately $(10 \div 20)$ %.

3.2 LHCf-ATLAS common physics program

Similarly to the last LHCf runs in 2015 and 2016, the common LHCf-ATLAS data taking will be implemented integrating the LHCf final trigger signal in the ATLAS Level1 trigger logic. The joint analysis of 13 TeV $p+p$ data taken in 2015 with ATLAS is on-going, and the first result has been published as a conference note [10]. In addition to the common operation with the ATLAS central detector, common operations with ATLAS ZDC and roman pot detectors are planned in the next operation.

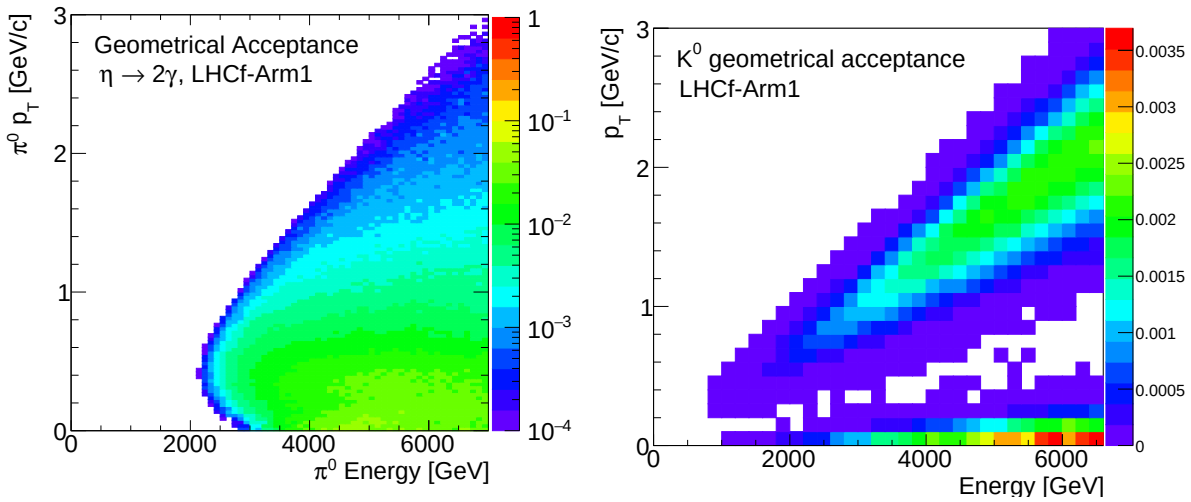

Figure 11: Left: geometrical acceptance of the LHCf-Arm1 detector for the detection of (left) photon pairs from η decays and (right) four photons from K^0 decays.

3.2.1 LHCf and ATLAS central detector

Combining the LHCf measurements with simple information from the central ATLAS detector, more detailed studies of forward particle production are performed, based for example on the selection of different production processes. Selecting events with no charged particles detected in the ATLAS region covering the pseudo-rapidity range $|\eta| < 2.5$, low mass diffractive events with mass smaller than 50 GeV can be well identified. The forward photon production cross-section in such events was measured in 13 TeV $p + p$ collision data obtained in 2015 [10]. Another measurement involving hadron production and exploiting the correlation between the central and forward regions is proposed in [16]. To verify the different phenomenological approaches implemented in the hadronic interaction models, this study requires measuring the forward neutron and π^0 energy spectra with the LHCf detector as a function of the number of charged particles identified in the central region with the ATLAS tracker.

3.2.2 LHCf and ATLAS ZDC

For the eventual LHCf activity in Run 3 the possibility to have common data taking with ATLAS also including the ZDC system is being evaluated. Combining the LHCf measurements with the measurements from the ATLAS ZDC hadron calorimeters, located behind the LHCf detector, the energy resolution for neutrons can be sensibly improved. Because the thickness of the LHCf calorimeters (corresponding to approximately 1.6 interaction lengths) is not enough to contain hadronic showers, many particles produced inside the LHCf towers leak out from the detector and hit the ZDC modules, located downstream of LHCf. Adding up the energy deposits measured both in LHCf and ZDC, the energy resolution for hadronic showers is expected to im-

prove from 35÷40% to 20%. The impact point of neutrons can instead be measured accurately by LHCf thanks to position sensitive layers which allow reconstructing the center of the showers with a position resolution of about 1 mm.

The improvement of the energy resolution allows not only to improve the systematic uncertainties on the measurement of the energy spectrum of forward neutrons but also to study the collisions between protons and pions though the one-pion-exchange (OPE) process. In a OPE event, a proton interact with the pion cloud around the other proton, and emits a forward neutron ($p + p \to p + n + \pi^{+*} \to n + X$) [17]. The contribution of OPE processes on the total forward neutron production depends on the energy and p_T of neutrons. A better energy resolution therefore implies a better performance in selecting OPE events by tagging the forward neutrons.

3.2.3 LHCf and ATLAS Roman Pots

A first tentative common operation with the ATLAS ALFA detector was performed in the first physics fill of the LHCf operation in 2015. The duration was very short, around 1.5 hours. Due to a safety reason unfortunately ALFA could not be moved to the operation position and the attempt was abandoned. This first attempt was supported by several physics cases which can be considered when combining the LHCf data with the ALFA measurement of forward scattered protons. For example, single diffractive events are well identified by detecting the scattered proton in the roman pot detector located on the other side, with respect to IP1, of the LHCf detector measuring neutral particles. Additionally, exclusive measurements of Δ resonance, $p + p \to p + \Delta \to p + p + \pi^0$, and the bremsstrahlung process [18], $p + p \to p + p + \gamma$, can be addressed by this common operation.

The acceptance of the roman pots has a strong dependence on the beam optics. The default LHCf operation conditions with the non-zero crossing angle and β^* of about 10 m does not fit the best conditions required for the roman pots, which require zero-crossing angle and very high β^* instead. Some tentative configurations have been simulated to understand the possible acceptance in different configurations. In case of $\beta^* = 90\,\text{m}$ and a total crossing angle of $100\,\mu\text{m}$, the ALFA roman pots have signals in 28% of the LHCf triggers, approximately, thus giving the possibility to collect a significant number of events during the eventual short LHCf run.

An optimization study of the beam optics for an eventual common operation is on-going.

4 Physics program with $p + O$ collisions at $\sqrt{s_{NN}} = 9.9\,\text{TeV}$

As in case of the previous $p + Pb$ collisions produced at the LHC, the asymmetry of the proton-Oxygen ion collision leads to important differences in the events observed by

the LHCf detectors, depending on whether they are installed on the proton-remnant or ion-remnant side. The proton-remnant side remains the most interesting from the point of view of CR physics, because on this side we can measure in principle all the particles that are emitted in the very forward region, once we translate the event back to the laboratory frame where the ion is at rest. Due to the magnetic systems located upstream, the LHCf detectors measure the neutral components produced in the collisions, mainly photon and neutral pions, achieving very precise measurements of their energy and transverse momentum. Neutrons can also be measured, although with lower precision due to the limited depth of the calorimeter ($44X_0$, $1.6\,\lambda_I$). Results on forward neutrons are very important for understanding the inelasticity of collisions, defined as the fraction of the energy that is transferred, following an inelastic hadronic interactions, to particles others than the leading baryons. This is an important point for the interpretation of CR data. The ion-remnant side is also significant, because on this side we find all the debris produced in the breakup of the nucleus and therefore the nuclear fragmentation region can be studied in some details. Differently from the $p + Pb$ case, in case of Oxygen ions particle multiplicity on the ion remnant side is not dramatic and makes it possible to run the detector with some forethought.

A simulation in these two different configurations has been implemented, considering the Arm2 detector geometry, to verify the feasibility of the measurement and the quality of the expected results. Two hadronic interaction models have been used for this simulation to generate collision products, QGSJET II-04 and EPOSLHC. A total of 10^7 events have been generated for each model, considering a 7 TeV proton hitting a 3.5 TeV/nucleon Oxygen ion with no crossing angle and random impact parameter.

The basic physics program foreseen in case of p+O collisions is similar to that foreseen for $p + p$ collisions. The important differences between the two cases, which must be considered to define the detector running configuration, are related to the hit multiplicity and ultra-peripheral e.m. collisions (UPC).

In section 4.1 the results of the simulation are presented and some comparisons of predictions given by the two hadronic interaction models, already in the post-LHC era, are shown.

4.1 Proton remnant side

Proton remnant side is the most favourable for the LHCf measurements. This is basically due to the low multiplicity of hits that is expected on this side.

Paragraph 4.1.1 shows the hit multiplicity levels expected on the proton remnant side. In paragraph 4.1.2 UPC are presented and the modification of particle spectra generated in hadronic interactions are discussed.

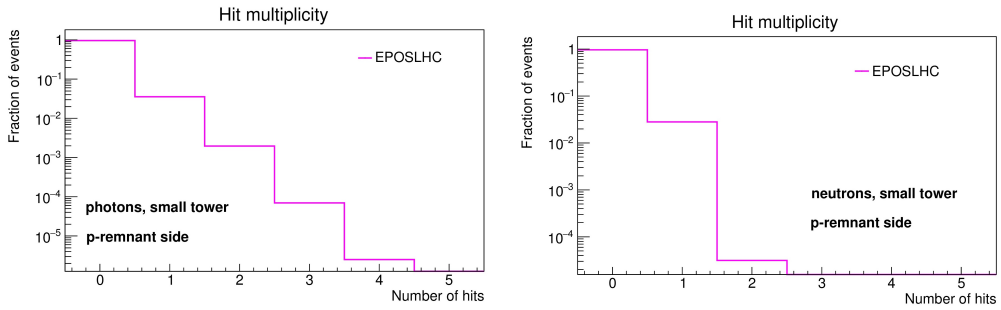

Figure 12: Multiplicities of photons (left side plot) and neutron (right side plot) hits in the small tower on the proton-remnant side.

4.1.1 Hit multiplicities

Due to the geometric configuration of the LHCf calorimeter towers, the highest particle hit multiplicity is expected on the small tower, i.e. the one which is usually positioned on the beam line.

Multiplicities of neutral particles hitting the small calorimeter tower of the LHCf detector located on the proton-remnant side are shown in figure 12. The distributions in this figure, obtained using the EPOSLHC model, refer to photons (left) and neutrons (right). The fraction of events with multiple hits is sufficiently low to allow measuring single particle events. Events with two hits in the small tower are of the order of 10% of the total events and can be identified and studied separately thanks to the good performance of the tracking modules used to measure the transverse shape of the showers developing inside the calorimeter towers.

4.1.2 Ultra Peripheral Collisions

When the impact parameter of a proton-ion collision is greater than the sum of the proton and nucleus radii, an Ultra Peripheral Collision (UPC) can occurs: a virtual photon from the strong electric field generated from the nucleus can interacts with the colliding proton. The LHCf detector has not the possibility to discriminate between a QCD-induced collision from an UPC-induced one so, in order to get the QCD component, the subtraction of the UPC contribution can be done only relying on a simulation. UPC simulations are performed using the STARLIGHT Monte Carlo code [19, 20] to simulate the virtual photon flux and either SOPHIA [21, 22] or DPMJET [15, 23] models to simulate low ($E_\gamma < 6$ GeV) and high ($E_\gamma > 6$ GeV) energy photon-proton collisions, respectively. Optionally, DPMJET can be replaced by the PYTHIA [24, 25] generator. In proton-lead collisions at $\sqrt{s_{NN}} = 5.02$ TeV UPCs generated more than half of the observed π^0 events [26].

In $p + Pb$ collisions at $\sqrt{s_{NN}} = 8.16$ TeV MC simulation studies predict an UPC contribution on photon and neutron spectra comparable or greater than QCD compo-

nent. Examples of UPC contribution expected in photon and neutron spectra in the very-forward region in $p + Pb$ collisions at $\sqrt{s_{NN}} = 8.16$ TeV are shown in figure 13. These simulations predict that the UPC contribution can be of the same order or much

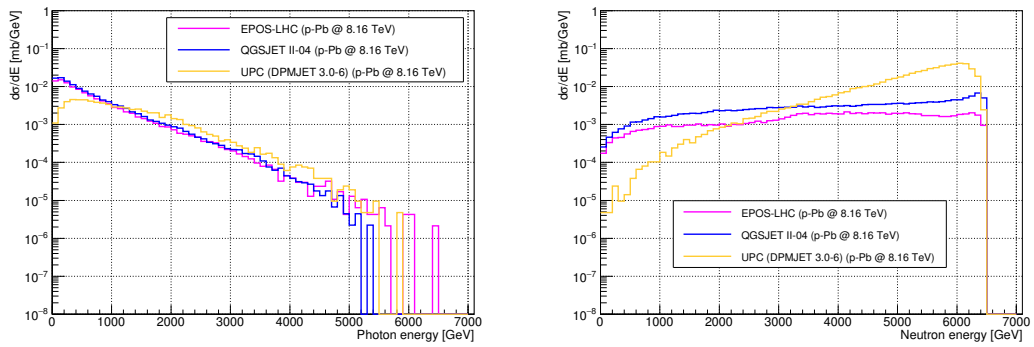

Figure 13: Energy spectra predicted by UPCs in $p+Pb$ collisions at $\sqrt{s_{NN}} = 8.16$ TeV compared with the predictions of EPOS and QGSJET hadronic interaction models. Left: photon spectrum for pseudorapidity $\eta > 10.94$. Right: neutron spectrum for $\eta > 10.76$

larger than QCD contribution in $p + Pb$ collisions.

In proton-Oxygen collisions the UPC contribution is expected to be much smaller since the virtual photon flux is proportional to Z^2. Figure 14 shows the predicted UPC energy spectra of photons and neutrons in $p + O$ collisions at $\sqrt{s_{NN}} = 9.9$ TeV compared with the QCD ones. $p+O$ simulations predict an UPC contamination at the

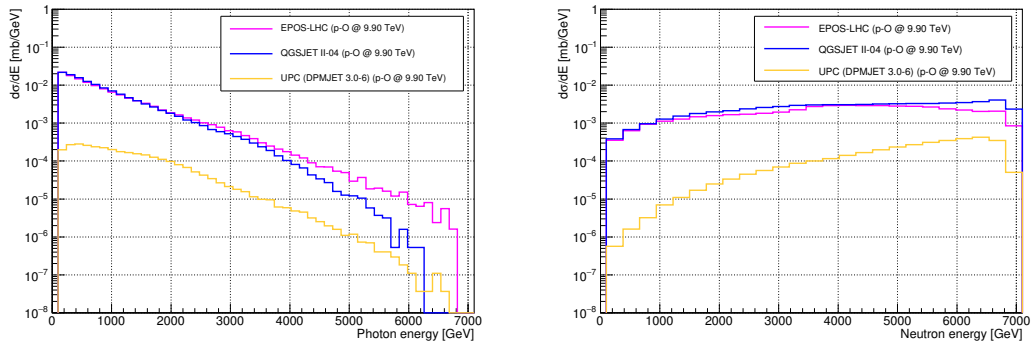

Figure 14: Energy spectra predicted by UPCs in $p + O$ collisions at $\sqrt{s_{NN}} = 9.9$ TeV compared with the predictions of EPOS and QGSJET hadronic interaction models. Left: photon spectrum in LHCf small tower. Right: neutron spectrum in LHCf small tower

level of few percents for both photons and neutrons (only excluding the high energy region at $\eta > 10.76$ for neutron). Proton-oxygen collisions give therefore the possibility

to study nuclear effects in high energy proton-ion collisions with a significantly lower background from UPC events with respect to the $p + Pb$ case. In order to compare the experimental results with the prediction of the hadronic interaction models, the UPC component must be subtracted from the measured data; as a consequence the uncertainty on the UPC simulation contributes to the systematic uncertainty on the final measurement. UPC simulations has an intrinsic 10% uncertainty for the virtual photon flux predicted by STARLIGHT, while another systematic uncertainty comes from the model used in the interaction between the photon and the proton; the second one was estimated comparing the UPC spectra predicted using DPMJET and PYTHIA generators. Figure 15 shows the estimation of the change in the total systematic error of the photon spectrum in $p + Pb$ collisions at $\sqrt{s_{NN}} = 8.16$ TeV after subtracting the UPC component and adding UPC systematic uncertainty. The systematic error estimation is based on the preliminary photon analysis of LHCf data taken during the $p + Pb$ run in November 2016. As shown in the picture, the UPC uncertainty has a

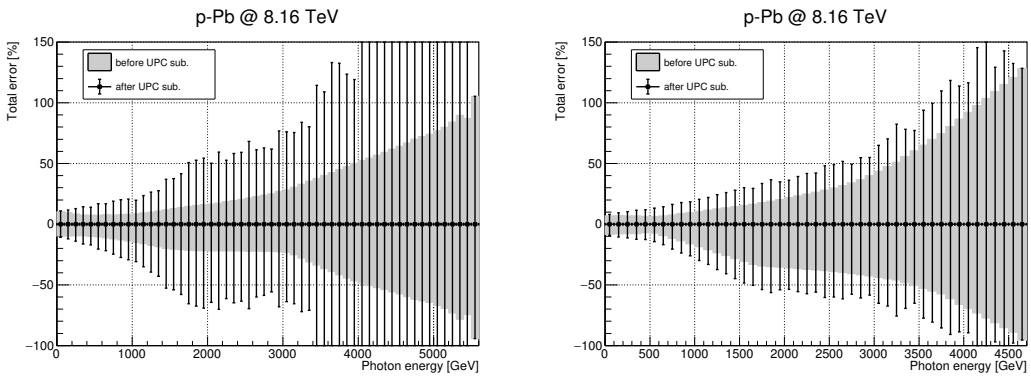

Figure 15: Estimation of the total (statistic + systematic) relative error of the photon energy spectrum in $p + Pb$ collisions at $\sqrt{s_{NN}} = 8.16$ TeV. Grey area represents the uncertainty before UPC subtraction, while black error bars show the total error after subtracting the UPC component. Left: $\eta > 10.94$. Right: $8.81 < \eta < 8.99$

huge impact on the overall systematic error in LHCf $p + Pb$ measurements.

Figure 16 shows instead the estimated change in the total systematic error of the photon spectrum in $p+O$ collisions at $\sqrt{s_{NN}} = 9.9$ TeV due to the UPC subtraction. In $p+O$ the contribution of the UPC uncertainty to the total error is negligible because of the very low UPC cross section with respect to the QCD one, as oppose as the $p + Pb$ case. Taking data in $p + O$ collisions will therefore strongly reduce the uncertainty associated to the UPC subtraction with respect to the $p + Pb$ case and it will give the opportunity to perform much more precise measurements on high energy p-ion collisions.

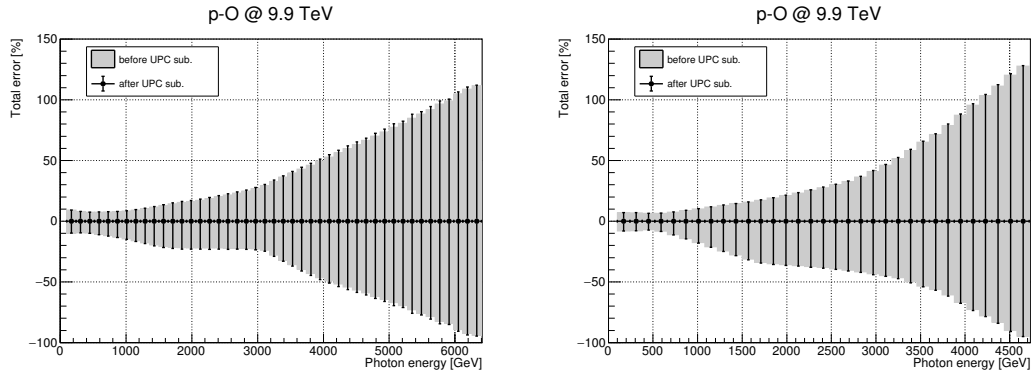

Figure 16: Estimation of the total (statistic + systematic) relative error of the photon energy spectrum in $p + O$ collisions at $\sqrt{s_{NN}} = 9.9$ TeV. Grey area represents the uncertainty before UPC subtraction, while black error bars show the total error after subtracting the UPC component. Left: $\eta > 10.94$. Right: $8.81 < \eta < 8.99$

4.2 Ion remnant side

4.2.1 Hit multiplicities

In analogy to the case of the proton-remnant side (figure 12), the multiplicities of photons and neutrons hitting the small calorimeter tower of the LHCf detector located on the ion-remnant side, evaluated with the EPOSLHC model, are shown in figure 17.

The left plot refers to the photon component, while the right one refers to neutrons. The fraction of events with multiple hits is clearly too high to allow measuring single particle events with the detector in the nominal neutral position. The lower plots in the same figure show how the multiplicities on the small tower reduce after moving the detector 15 mm upward, in such a way to reach safe position slightly out of the beam center.

4.3 Notes on O+O collisions

The same offset of the detector position from the beam center can be considered to reduce the hit multiplicity to an acceptable level in an eventual O+O run. This type of collision is also very interesting from the point of view of cosmic-ray physics, because it also represents a process really happening in the atmosphere, even if with a lower frequency with respect to $p + O$ collisions.

A measurement in the LHC forward direction for collisions between light ions is of interest to model developers, as recalled by T. Pierog of KIT in a recent presentation at the CERN Council Open Symposium on the Update of European Strategy for Particle Physics (13-16 May 2019 - Grenada, Spain) [12]. If the $p+O$ run could not be done, the LHCf Collaboration will be therefore interested to take data in O+O collisions, trying to collect enough data to replicate the basic studies done so far at least for photon,

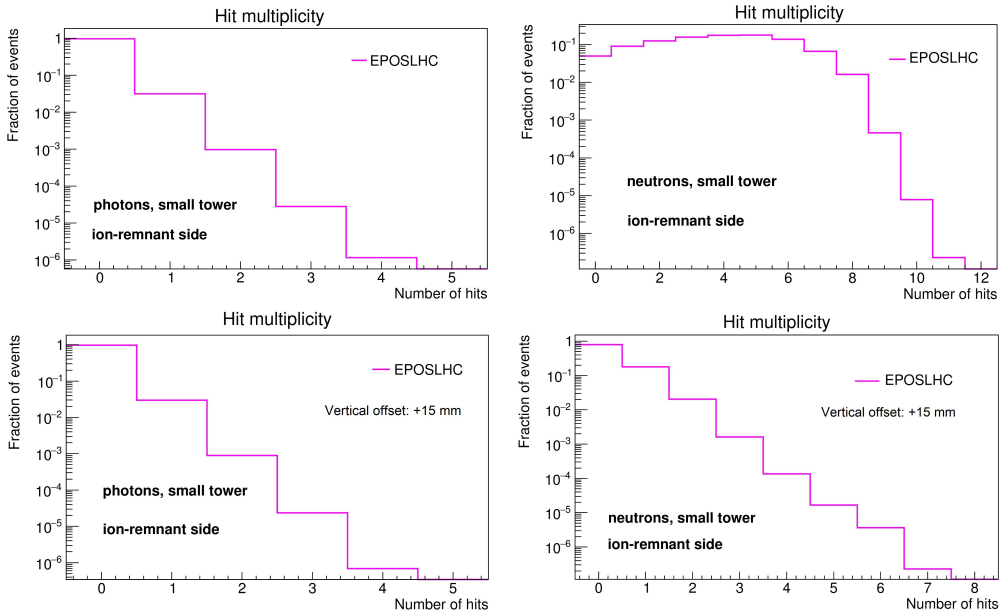

Figure 17: Multiplicities of photons hits (left side plots) and neutron hits (right side plots) in the small tower on the ion-remnant side. Top plots refers to the nominal detector position with the small tower accessing the beam line. Bottom plots shows how the multiplicity distributions are modified moving the detector 15 mm upward, slightly out of the beam line.

neutron and neutral pions.

5 Status of detectors and installation issues

5.1 Hardware setup for the proposed measurements

The LHCf experiment is based on two similar detectors, i.e. two electromagnetic sampling calorimeters, made of plastic scintillator and tungsten layers, complemented by a tracking system. Each detector, called Arm1 and Arm2, is composed of two independent calorimeter towers enclosed in a single box that contains also some part of the front-end electronics. Detailed information about these detectors can be found in references [27, 28, 29]. During data taking in the default configuration the detectors are positioned in such a way that one of the calorimeter towers, the smallest one, lies directly along the beam line at zero degrees. The LHCf standard run setup, used in the past and foreseen also for the 14 TeV pp run, requires the installation of both detectors inside the reserved slots of the two TAN absorbers located 140 m on opposite sides of Interaction Point 1 (IP1). The Arm1 detector is located between IP1 and IP8, while the Arm2 detector is located in between IP1 and IP2. This allows a comparison of the results between the two detectors and also the study of double diffractive events.

Although it is important to consider these aspects, in order to minimize the impact on the ATLAS ZDC physics program during the $p + O$ run, LHCf could be eventually operated as a single arm detector, installing only the Arm2 detector in the TAN absorber located between IP1 and IP2 (LSS1R side). In this way a "single-arm" configuration, which has been already used for the 2013 and 2016 $p + Pb$ collisions, would be used instead of the usual one. The choice of the Arm2 detector is preferred because of its better spatial resolution. With respect to Arm1, Arm2 exploits the excellent spatial resolution of eight micro-strip silicon sensors arranged, as X/Y layers, at four different depths inside the calorimeter. These silicon detectors are used for the reconstruction of the transverse shape of showers developing inside the calorimeter and are therefore critical for the measurement of the impact points and for the identification of multiple hits and particle type. Moreover they can also independently measure the energy released in the calorimeter with a good enough resolution, as demonstrated in [29], and can therefore be used to monitor the stability of the energy measurements performed by means of the scintillator system.

In case of a "single-arm" run, the detector must be installed preferentially on the proton-remnant side. The usual beam configuration with proton in Beam 1 and ions in Beam 2 is compatible with the installation of the Arm2 calorimeter in the LSS1R zone. In any case the run of LHCf for p+O collisions requires data taking on the proton-remnant side as the primary choice. Beam swap could also be a possible choice.

5.2 Hardware upgrade

A few years ago both the Arm1 and Arm2 LHCf detectors underwent a major upgrade phase to satisfy better requirements in terms of radiation hardness and to correct some minor problems in the custom electronics.

All plastic scintillator tiles of both detectors were replaced with GSO tiles and all plastic scintillator fibers of the Arm1 tracking system were replaced using GSO fibers. FOr the Arm2 detector all the microstrip silicon modules (silicon sensors and front-end circuitry) were replaced by completely new ones, manly to implement a different wire bonding scheme, thus allowing to move the saturation effect of the front-end chips to higher energies.

Currently a major upgrade of the Arm2 silicon DAQ electronics is required. The motivations of this need are basically the aging of the silicon DAQ electronics, which is installed on top of the TAN absorber in the LHC tunnel, the lack of replacements for the most of the currently installed devices (FOXI optical transmitters and receivers, derived from the LEP experiments, the old and sophisticated control ring developed for the CMS experiment, including the FEC, TSC, DOHM modules, and so on). Furthermore the Arm2 silicon DAQ system gives currently the largest contribution to the total DAQ dead time. The new DAQ scheme will allow reducing this contribution of a factor of 10, thus making it negligible with respect to the other contributions.

Concerning the Arm1 detector, which is already capable to sustain a 2 kHz DAQ

rate, an electronics upgrade is not required. Only the recovery of the original mechanical configuration, modifiedfor a ruh at the RHIC accelerator (RHICf experiment), is required,

5.2.1 Upgrade of the Arm2 DAQ system

The detector read-out and control electronics (both the part in the LHC tunnel and the back-end part in USA15 cavern) will be upgraded, according to the following motivations.

- Substitute aged electronics: the employed electronics is aged (> 10 years) with high irradiation sustained by the boards installed in the tunnel area during data taking.
- Speed-up the read-out of at least one order of magnitude, thus significantly reducing the contribution to overall dead-time.
- Simplify and optimize the slow control system, instead of using and adapting the complex CMS "control ring" architecture as in the previous implementation.
- Employ standard and modern commercial devices (instead of custom and dated ones), taking care that they are characterized by suitable radiation hardness with respect to expected radiation in the operation area (i.e. on top of the front part of the TAN structure).

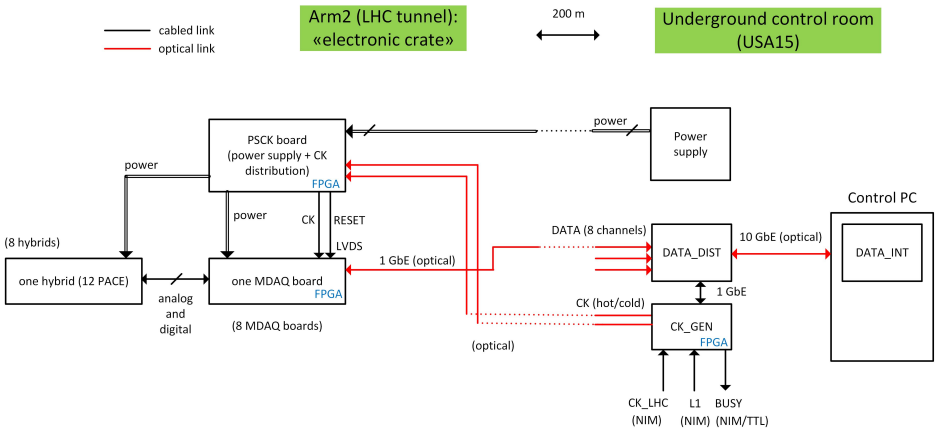

Figure 18: Block scheme of the new electronics for Arm2 detector.

The main modifications of Arm2 read-out and control architecture are listed in what follows (see figure 18). In the tunnel area, these modifications imply substituting the read-out and control boards in the electronics crate, which is installed on top of the TAN structure, while no modifications are needed on the front-end hybrid boards

contained in the detector structure. On the back-end side (USA15 cavern) the whole read-out and control system will be upgraded. The already installed optical links between tunnel area and USA15 cavern will be employed (unless they are found to be out of specifications because of the absorbed radiation).

- The event data transmission from the read-out MDAQ boards (custom-designed boards at Arm2 location) to the control PC (USA15 cavern) will be operated with standard optical 1 GbE (1 Gbps Ethernet) protocol, which substitutes the previously employed FOXIchip protocol characterized by 100 Mbps peak speed. The dead time contribution is thus reduced by a factor $\sim$10: in fact with the previous implementation, the event read-out dead time was $\sim$1 ms, while with the new one it is expected to be order of tens of μs. On the MDAQ boards, the optical FOXIchip transmitters will be substituted by standard SFP GbE optical modules. On the back-end side (USA15), the previously employed custom VME-standard data receiver board, with FOXIchip receivers, will be replaced by a standard optical switch (DATA_DIST) and a 1 GbE PCI express board (DATA_INT) installed in the Arm2 control PC. The DATA_DIST switch is interfaced with the 8 MDAQ sections through 1 GbE optical links, while it is interfaced to the DATA_INT board via a single 10 GbE link, thus avoiding additional dead time during serialization of the parallel streams of event data coming from the MDAQ sections.

- The slow control system of MDAQ boards and PACE3 front-end chips will be implemented on the same GbE bidirectional link discussed above; this is a great simplification with respect to the previous implementation, which employed several custom boards originally designed for the CMS apparatus (FEC and TSC boards on back-end side, DOH and CCU boards on front-end side, linked each other in a redundant control ring). The I^2C slow control interfaces required by PACE3 chips will be managed by the MDAQ FPGA (previously they were managed in the CCU boards).

- The generation of fast signals (L1 trigger, CALIB, RESYNC) for PACE3 chips will be done is a similar fashion to the previous implementation, i.e. by encoding them on the back-end side in the 40 MHz LHC clock signal (as different sequences of missing clock cycles) and by decoding them on the read-out MDAQ boards. The corresponding electronics (relatively simple PLL circuits) will be custom designed, while in the previous implementation PLL-based circuits, designed for CMS apparatus, were employed (these circuits are more complex than needed for LHCf apparatus).

  On the back-end side, the custom-made PLL-based board (CK_GEN) will be connected to the control PC via GbE link and also receive the incoming LHC clock line; the 40 MHz clock with encoded fast signals is then sent from CK_GEN board to the tunnel area via dedicated redundant hot/cold optical link.

In the Arm2 electronics crate a decoding PLL-based circuit will be implemented in a new dedicated section of the power control board (PSCK board): this circuit will determine the currently active link between the redundant hot/cold ones and will distribute the corresponding line to all the MDAQ boards located nearby, via LVDS links. A similar PLL-based circuit will be present on each MDAQ board for final decoding of fast signals and LHC clock reconstruction (the LHC clock is also sent to the PACE3 hybrid front-end boards).

- The number of independent MDAQ sections will be doubled (from 4 to 8, i.e. one per each side of the 4 detector modules) thus doubling the segmentation of the system; this, together with the redundant link for LHC clock with encoded fast signals, will balance the removal of the redundant control ring made with DOH and CCU boards in the previous implementation.

- The FPGA family to be employed in the new MDAQ, PSCK and CK_GEN boards has been selected as the Xilinx Zynq 7000 SoC, featuring a free TCP/IP GbE controller without the need to use the full internal CPU architecture. This FPGA family has been successfully characterized for radiation hardness (both total absorbed dose up to 2 Mrad and single event effects for LET up to 17 MeV/(g cm^{-2})) and is compatible with employment in the TAN area during Run 3. This FPGA will make it possible to avoid the use of external FIFO chips (necessary in the previous MDAQ implementation with Altera Cyclone I FPGA).

- In the new MDAQ board, a 14-bit ADC model will be employed for digitization of PACE3 output signal (it was 12-bit in the previous implementation), thus increasing the measurement resolution.

5.2.2 Arm2 upgrade planning and status

Preliminary tests to verify the feasibility of the proposed upgrade have been already performed, by using a Xilinx ZC702 evaluation board equipped with Zynq 7020 FPGA.

- The proposed TCP/IP GbE data link has been tested successfully, between the ZC702 evaluation board and a standard office PC with standard cable connection. The effective data transmission speed measured was 940 Mbps (92% of nominal maximum bit rate).

- The proposed management of slow control I^2C interface between MDAQ and PACE3 chips via MDAQ FPGA (instead of CCU board) has been tested, by implementing successful read/write operations of PACE3 internal registers via the ZC702 evaluation board with a standard I^2C logic module implemented in the Zync 7020 FPGA.

The next steps in the development of the electronics upgrade are listed below.

- Test of GbE data link in the complete back-end configuration: industrial PC with internal 10 GbE board (DATA_INT), connected to the switch (DATA_DIST), in turn connected with the ZC702 evaluation board (emulating the MDAQ board). All the above listed items are standard commercial ones and have been already procured. This test will be carried out by the end of July 2019.

- Development of the new software to manage slow control and event read-out with the new back-end system.

- Development of the new custom boards (MDAQ, PSCK and CK_GEN). The main task here is the design of the circuit containing the new Zynq 7000 FPGA.

  The active electronics parts for new custom boards have been already selected, by requiring a minimum qualification for radiation hardness (immunity for absorbed dose > 100 krad, SEU cross-section $< 10^{-6}$ cm^2/bit), even if stray radiation conditions on Arm2 electronics crate (on top of TAN) are expected to be better than that during Run 3. The complete definition of the control system and DAQ specifications is expected to be completed by the end of July 2019, while the production of the first prototype of the MDAQ board is foreseen by the end of September. The final scheme of this board will be finalized by the end of 2019 and at the beginning of 2020 the final production will start. The design of the last two boards, PSCK and CK_GEN is currently ongoing. The first prototypes should be ready by the end of Jul 2019.

- Development of the rest of the FPGA firmware. For MDAQ boards, it will be possible to employ most of the custom VHDL code already developed for the previous implementation, while few completely new code will be needed for PLL-based circuits and ADC interfaces.

5.3 Trigger logic upgrade

An upgrade of LHCf trigger logic will be performed to efficiently collect events with high energy π^0 and η in a higher-luminosity operation condition with $p + p$ collisions in LHC-Run3. Assuming for the luminosity a value of $10^{30}\text{cm}^{-2}\text{s}^{-1}$, the simple event rate with any showers in the calorimeters exceeds 10 kHz, which is much higher than the maximum DAQ rate even after the upgrade of Arm2 read-out system. Therefore, we will introduce the special triggers, Type I Pi0 Trigger and High EM Trigger, as well as Shower Trigger, which are dedicated for detection of type I π^0 and η, and type II π^0 events, respectively. All trigger signals will be formed in the VME trigger board, containing a programmable FPGA (CAEN V2718), starting from the 32 hit pattern signals corresponding to the energy deposits in the 32 scintillator plates, discriminated with a variable threshold in each detector.

- **Shower Trigger:** this is the LHCf basic trigger mode to detect any shower events in the calorimeters. These trigger signals are generated when any successive three

layer hits in each calorimeter tower are detected. The threshold are set to a signal level equivalent to an energy deposit of 0.5 GeV in each scintillator layer, except the sixth layer of each tower, whose threshold is set to a higher value for High-EM trigger, as discussed below. The hits of these high-threshold layers are not considered in shower trigger logic, and the hits of sixth layer are always treated as ON. From simulation we know that the trigger efficiency is 100% for photons with energies above 200 GeV and about 70% for neutrons with energies above 1 TeV.

- **Type I π^0 Trigger:** this is a special trigger mode to detect Type I π^0 events, in which both calorimeter tower simultaneously detects one photon from π^0 decays. Type I π^0 Trigger has already been introduced in the past LHCf operations, and worked successfully. This trigger is issued when shower triggers are generated in both the calorimeter towers. To reduce the contamination of hadronic showers, only the hit pattern signals of the first seven layers are considered for shower detection. As already described for the shower trigger logic, the hit of the sixth layer is always set to ON. The trigger efficiency for the Type1 π^0 events is expected to be 98%. This trigger works efficiently also for η meson detection, since the events generated by η are topologically similar to the type I π^0 events.

- **High EM Trigger:** this is a newly introduced trigger, focusing on the detection of high energy photons and type II π^0 events. In type II π^0 events, photon pairs from π^0 decays hit the same calorimeter tower and induce high energy electromagnetic showers, which are equivalent to photon induced showers with energies above 2 TeV and 1 TeV, for the small and large tower respectively. Requiring a hit on the sixth layer with relatively high threshold, equivalent to the energy deposit of 10 GeV and 6 GeV, type II π^0 events are enriched in the triggered samples, togehter with high energy photon events. The trigger efficiency of type II π^0 events is exepected to be 97%. This High EM Trigger was originally designed for the RHICf experiment [30], a very forward experiment at BNL-RHIC that has been realized with the LHCf-Arm1 detector, and it successfully worked to detect many type II π^0 events.

The final trigger signals are generated combining these three trigger signals, after some prescaling on the shower trigger to reduce its rate. The overall trigger performances and rates have been studied by using an available event sample of the full detector simulation with the QGSJET2 model at $p + p$, $\sqrt{s} = 13$ TeV. The trigger rates of Shower, Type I π^0, High EM Triggers are 10.5 kHz, 320 Hz, and 840 Hz, respectively. Applying a prescale factor of 14 to the Shower Trigger signals, the total final trigger rate is expected to be 1.9 kHz. Considering the event-by-event dead time for the read-out of data, the recorded event rate becomes 950 Hz (with an efficiency of 50%). Table 2 shows a summary of the various triggers and of the expected event rates.

	Trigger mode	Trigger rate	Recorded rate	Events in the record
Arm1	Shower	10.5 kHz	375 Hz	γ: 135 Hz, neutron: 110 Hz
	TypeI π^0	320 Hz	160 Hz	typeI π^0: 24 Hz, η: 0.2 Hz
	High EM	840 Hz	420 Hz	typeII π^0: 40 Hz
Arm2	Shower	11.5 kHz	405 Hz	γ: 140 Hz, neutron: 120 Hz
	TypeI π^0	980 Hz	490 Hz	typeI π^0: 33 Hz, η: 0.2 Hz
	High EM	970 Hz	485 Hz	typeII π^0: 50 Hz

Table 2: The rates of trigger signals and recorded events for LHCf Arm1 and Arm2 detectors with a luminosity of $10^{30}\text{cm}^{-2}\text{s}^{-1}$. The DAQ efficiency is assumed to be 50%. The prescale factor for Shower Trigger has been set to 14.

The limitation of DAQ rate comes from the dead time of the readout system, that will be around $400 \div 500\,\mu$s for both detectors.

The optimal condition is to set the trigger rate approximately equal to the maximum DAQ rate, i.e. around 2 kHz. This can be achieved accepting the full 300 Hz pion event rate, the full 800 Hz high energy e.m. event rate and prescaling the dominant single showers event rate down to 900 Hz (Arm1). The readout rate and efficiency are 1 kHz and 50% in this case (estimated from MC study). The prescale factor 14 has been calculated according to a study with full detector simulation at 13 TeV pp.

5.4 Beam tests at SPS

The LHCf collaboration is requesting for dedicated beam tests at SPS for re-calibrating the detectors and testing the whole hardware setup with particle beams before the eventual $p+p$ and light ion runs. In the beam tests electron, proton and muon beams will be fired into both Arm1 and Arm2 detectors, changing the momentum and the impact position of the beams (Tab. 3). Electron and proton beams induce electromagnetic and hadronic showers, respectively. The obtained data will be used, as in the past tests, for the energy calibration of the calorimeters and for the study of the impact point reconstruction using the position sensitive layers. Although any significant degradation of the detector performance due to aging and radiation damage is not expected, a careful calibration with about 2% level precision is necessary just before the LHC operation to minimize the systematic uncertainty of the energy scale, which is dominant in the systematic uncertainty of the energy spectrum measurements. The DAQ system developed for the LHC operations will be used for the beam tests also. The whole system including the new Arm2 silicon readout system and the new trigger logic will be tested in the beam test as well.

Considering the operation schedule of the $p+p$ and $p+O$ runs, the beam test schedule will be fixed. Basically a beam test is performed 1-2 month before an operation at LHC and takes 10 days or 6 days to complete the test including the setup and removal time with all of or one of the Arm1 adn Arm2 detectors, respectively. In the case that

the $p+p$ run is scheduled for the very beginning of LHC Run3 and the LHCf detectors are installed before the LHC restart, there is no time slot for a beam test because SPS restarts simultaneously with the LHC restart. Only in this case, a beam test at SPS need to be performed after the LHC operation, and an additional beam test using other beam facilities like Frascati in Italy is considered for initial calibration and a test of new silicon readout system. In other cases like the LHCf detector installation in the first technical stop in 2021, the beam test schedule can be relatively flexible. Another beam test is performed before the $p+O$ run expected in 2023.

Table 3: Specifications of the beam test at SPS.

Beam conditions	electrons, 100 - 200 (or more) GeV/c protons, 350 GeV/c and muons
Duration	10 days for two detectors, 6 days for one detector (2 day for setup and removal in the beam line 4 days for one detector.)

5.5 Installation requirements

5.5.1 Radio-protection issues

The installation procedure of both LHCf detectors in the LHC tunnel was defined in details before the first run and successively largely improved before the $p+Pb$ run in 2012, with the purpose of minimizing the total requested time and the expected doses for the involved team. All the electronics and mechanics to be placed in the tunnel were assembled in laboratory at ground level using a unique strong base plate holding together all the different parts of the apparatus, thus making it possible to carry out most of the cabling before the final transportation of the instrument to underground. The most updated documentation concerning the installation of the Arm2 detector can be found on the CERN EDMS system (https://edms.cern.ch/document/1728748/1.0). For Arm1 the installation procedure is the same apart from minimal differences in the final cabling.

The upgraded Arm2 apparatus will not present significant differences with respect to the previous implementation, from the point of view of the installation procedure: the custom-made boards in the Arm2 electronics crate will be replaced with newly designed ones, without impact on the overall structure, while the number of optical links between the electronics crate and the USA15 cavern will increase from 12 to 18.

The main operations to be carried out underground for each detector are the following: (i) transportation of the detector, by means of a dedicated trolley, from the underground lift to the installation locations (the TANs, located 140 m from IP1), and removal of few cable ties fixing the detector to the trolley; (ii) setup of the remote control system in the corridor between lift and tunnel (operation independent from

the others); (iii) remotely controlled transportation of the detector from the trolley to inside the installation slot; (iv) cabling and fixing of the detector. In particular operations (i), (iii) and (iv) requires the presence of operators in the tunnel. A detailed list of the operations and the necessary manpower, already used for the $p + Pb$ run at the end of 2016, is reported in figure 19 to show which is the impact of the LHCf installation procedure and how long it may take. This table is being used by the CERN

	Operation	Time (minutes)	Required Personnel	Position	Individual Dose (μSv)	Collective Dose (man.μSv)
1	Bring downstairs the detectors and the tooling needed for the installation	10	2 physicists from LHCf	PM15-> UL14	0,0	0,0
2	Bring downstairs electrical cupboard, camera and desktop	20	2 operators from EN/HE	PM15-> UL14	0,0	0,0
3	Prepare/check mini-cranes for operation	15	2 operators from EN/HE	TAN and between TAN and UJ14	0,0	0,0
3 bis		5	2 operators from EN/HE	TAN (to install cameras)	0,7	1,3
4	Bring the shielding box	5	2 operators from EN/HE	Bunker in UJ13 ->TAN	0,3	0,5
5	Remove Cu bar and place it in the appropriate shielding box	10	2 operators from EN/HE	UJ14	0,0	0,0
6	Remove bar shielding box	5	2 operators from EN/HE	TAN-> bunker in UJ13	0,3	0,5
7	Bring the detector to the TAN	5	2 physicists from LHCf	UJ13 -> TAN	0,3	0,5
8	Install detector	10	2 operators from EN/HE	UJ164	0,0	0,0
9	Remove electrical cupboard and cameras from TAN	5	2 operators from EN/HE	TAN side	0,7	1,3
10	Bring upstairs electrical cupboard, camera and desktop	20	2 operators from EN/HE	UJ14 -> PM15	0,0	0,0
11	Screwing (no fine positioning)	15	2 physicists from LHCf	On top of the TAN	1,3	2,5
12	Installation of the Front Counter	10	2 physicists from LHCf	On top of the TAN and behind it on the footbridge	0,8	0,8
13	Cabling for preamp and FC	5	2 physicists from LHCf	On top of the TAN and behind it on the footbridge	0,4	0,4
14	Additional cabling for the electronics box	10	2 physicists from LHCf	On top and side of the TAN	0,8	0,8
15	Survey		2 technicians from RE/ARP	Around the TAN region max 60 minutes near the TAN)		
16	Electronics commissioning	60	2 physicists from LHCf	This test is performed from USA15. In case of problems 2 physicists from LHCf will have to work on top of the TAN for a period which depends on the kind of problem (typically 15-60 min)		
17	Mechanical commissioning (manipulator)	15	2 physicists from LHCf	Test performed mainly from USA15. Two physicists is required to stay near the TAN for about 15 minutes	2,0	2,0
18	Bring back detector shielding boxes	5	2 physicists from LHCf	TAN->PM15	0,3	0,3
19	Exit the zone	10	2 physicists from LHCf	TAN->PM15	0,0	0,0
	Total	240		**Collective Dose (man.μSv)**	TOT	11
				operators from EN/HE		4
				physicists from LHCf		7

Figure 19: required operations and necessary manpower for the installation of one LHCf detector; this table is being used by the CERN RP team to estimate the doses expected for operators who would take part in this activity. The total dose expected for single operator, shown in the last columns of the table, is calculated assuming to install the apparatus during the first technical stop foreseen for 2021. Estimated doses are lower than 10 μSv, similar to natural radioactivity.

radio-protection (RP) team for estimating the expected doses for the LHCf installation in Run 3. The last two columns report the doses expected in case the installation is carried out during the first technical stop foreseen in Run 3. According to these calculations the contribution given by activated materials is of the same order of the daily dose due to natural radioactivity. It should be considered also that the uninstall procedure is quite shorter than installation, because no commissioning is required. The

total uninstall procedure would take less than 3 hours for each detector.

After discussion with the CERN radiation protection team we confirmed that the above reported operations are compatible with the radiation environment in the relevant tunnel areas, expected both during the current Long Shutdown 2 and the beginnig of the next Run 3. Detailed calculations of the expected doses are on-going. The installation of the LHCf detectors in the early phase of Run 3 is therefore the optimal solution for a possible LHCf run with $p + p$ collisions, at least from the point of view of the safety for operators. In case of a later installation the level of radiation would be higher and this possibility has to be carefully evaluated with the radio-protection team.

During the installation procedure a geometric survey of the detector's setup is required, as foreseen also in the operation list reported in figure 19. LHCf need in fact a measurement by the CERN BE-ABP team (Beams Department - Accelerators and Beam Physics Group), which generally lasts approximately 1 h. This survey is necessary to determine precisely the position and orientation of the LHCf detectors in the LHC system and is required for the study of the detectors alignment with respect to the LHC particle beams. This measurement is completely independent from the beam crossing angle configuration that will be used during during an eventual LHCf run.

5.5.2 Commissioning

After the installation of the LHCf detectors into the LHC tunnel the detector's commissioning phase will start soon. Basic tests, such as a confirmation of the cable connections, will be quickly performed by checking the noise level on signal lines arriving in the USA15 counting room. A semiconductor laser, which was installed into a rack in USA15 for the last $p + p$ operation in 2015, will be available for these tests. The test procedure foresees the delivery of the laser light to the detectors via a optical fiber. The light pulses are then distributed to each PMT photocathode.

The trigger and readout systems will be tested by using dummy signals. The trigger module with a FPGA chip (CAEN V2718) will be use to generate dummy signals. The latency and frequency characterizing the generation of these dummy signals will be controlled via specific user commands, and the trigger logic will be tested with many signal patterns instead of PMT signals from the detectors.

Some commissioning works require beams. The most important one is latency measurement of signals, which is necessary for optimization of charge integration timings, and also for adjustment of latency of LHCf triggers sending to ATLAS. It takes about one hour. This work can be performed even before declaration of "STABLE BEAM". During the beam setup, the LHCf detectors stay at the safe position (about 8 cm up from the operation position). Even in the safe position, low energy particles generated in $p + p$ collisions hit the detectors and this measurement can be done withe these signals.

6 Requirements for the LHCf data taking in Run3

In this section we summarize the minimal requests of the LHCf collaboration for the two proposed runs with $p+p$ and $p+O$ collisions.

An important and general point valid in both cases concerns the beam crossing configuration. In fact the LHCf detectors are conceived to take data with null beam crossing angle or with downward going beams crossing in a vertical plane. A remotely controlled motorized system allows moving the calorimeters up and down to allow positioning the small tower on the beam collision line. In case of horizontal beam crossing, the projection at the LHCf position of the interaction line (i.e. the direction defining the infinite pseudo-rapidity limit) gets an offset along the horizontal direction and there is the risk not to be able to intercept it with the calorimeter, thus loosing the possibility to measure products of collisions emitted at extremely small angles and to reconstruct the zero-degree direction with sufficient spatial resolution.

The last documentation available on this point (see for example the recent presentation by N. Karastathis at the Evian 2019 workshop [31]) confirms that the "round" beam optics foreseen for the first year after the restart of the LHC in 2021, i.e. for the $p+p$ run, implies a vertical crossing plane with a nonzero crossing angle at the Interaction Point 1 (IP1), where LHCf is usually installed. Concerning the eventual run with light ions in 2023 the same optic foreseen for the $Pb+Pb$ run will be probably used and the same configuration with vertical beam crossing is still possible.

In paragraphs 6.1 and 6.2 we make an estimate of the expected pile-up effect and we discuss the beam parameters and the other minimal requests to complete the minimum physics program for the $p+p$ and $p+O$ runs.

6.1 $p+p$ run at $\sqrt{s} = 14$ TeV

For the $p+p$ run we have assumed an interaction cross section $\sigma_{\text{int}} = 80\,\text{mbarn}$, a nominal luminosity $\mathscr{L}_{\text{nom}} = 10^{30}\,\text{cm}^{-2}\text{s}^{-1}$ and a nominal number of bunches per beam $N_{\text{nom}} = 500$. We have also assumed a 7 TeV beam energy, but the following requests remains valid also in case of 6.5 TeV beam energy.

6.1.1 Pile-up effect

The event pile-up effect is in principle an issue for the LHCf measurement. It is in fact impossible for LHCf to distinguish a potential overlap of different collision events produced in the same bunch crossing. Therefore it is important to run with a low probability of interaction per bunch crossing. The mean interaction frequency for the single bunch is $\Delta N/\Delta t = [10^{30}\text{cm}^{-2}\text{s}^{-1} \times 8 \cdot 10^{-26}\text{cm}^2]/500 \simeq 160\,\text{Hz}$. Dividing this value by the revolution frequency of a single bunch we can derive the probability of one interaction in a single bunch crossing, $\lambda_{BC} \simeq 1.4 \cdot 10^{-2}$. This is low enough as not to present a real problem for the measurement, at least at this luminosity.

Beam parameters for the LHCf run with $p+p$ collisions at $\sqrt{s}$ =14 TeV	
Parameter	*Value*
Colliding bunches	~ 500
Minimum bunch spacing	200 ns
Luminosity ($\mathrm{cm^{-2}s^{-1}}$)	$\lesssim 10^{30}$
Inelastic cross section (mb)	80
μ (average n. of collisions per BC)	0.014
Beam crossing	vertical, downward
Beam crossing angle (μrad)	best: 290 (total)
β^* (m)	best: ~ 10 ($\gtrsim 1$)

Table 4: Summary of beam parameters proposed for $p+p$ collisions.

An additional and potentially critical limit for the detectors is represented by the time requested for the development of the signals produced by the scintillator system of the calorimeter. The fast signals from the PMTs [28] are sent to preamplifiers and then to the counting room through 200 m long BNC cables. At the end of these cables signals become wider because of the cable dispersion. The minimum time interval required between two consecutive signals to avoid their superposition after traveling through the long cables is approximately 500 ns. A 500 ns gate is used for signal charge integration to be sure to include this long tail. During this time interval we have 2.8 beam crossings, corresponding to an expected mean number of interactions $\lambda \simeq 2.8 \times \lambda_{BC} \simeq 0.039$. The probability to have one further interaction in this time interval and a corresponding signal in LHCf is, according to the Poisson distribution, $p \simeq 0.005$. Therefore signal superposition affects approximately 0.5 % of the events and does not represent a major issue. We can in fact easily identify these events and eventually remove them from the analysis.

Table 4 summarizes the proposed beam parameters for running the LHCf experiment with $p+p$ collisions at the highest energy. The best value of the total crossing angle from the LHCf point of view is around 290 μrad, configuration that maximizes the accessible phase space, but lower values are still acceptable. A not too small value of the β^* parameter is required to avoid event by event fluctuations in the beam center. This table has been already presented at tha CERN LPC meeting on 26 May 2019 and, according to the discussions with the coordinators the proposed values are not unreasonable, even if, as already mentioned, some of them need to be adjusted. Concerning the number of bunches, while 200 ns is the minimum requested bunch spacing, a slightly larger spacing using a smaller number of bunches could be acceptable if still maintaining the luminosity around $10^{30}\,\mathrm{cm^{-2}s^{-1}}$ and the pile-up at the level of percent.

6.1.2 Minimum physics program

The main purpose of LHCf in the p+p run at $\sqrt{s} = 14\,\text{TeV}$ is to collect a larger statistic data set, compared with the previous case at 13 TeV. According to the results of the 13 TeV run we estimate that a reasonable minimum number of registered π^0 events to produce new relevant physics results is of the order of 2.5×10^6, a factor 10 more than before. In particular the modeling of the region of the phase space for $p_t > 1\,\text{GeV}/c$, i.e. the transition region between soft and hard collisions, is not well established. The previous LHCf measurements present a large statistical uncertainty in this region. In general the pion spectra measured by LHCf at high energy ($x_F > 0.5$) and high transverse momentum ($p_t > 1\,\text{GeV}/c$) are dominated by the statistical uncertainty. The amount of data expected for the new run corresponds to an integrated luminosity of about $20\,\text{nb}^{-1}$ for a fixed detector position (nominal position). To further extend the accessible phase space, covering some rapidity interval that is not covered in the nominal detector position because of the non-standard geometry of the detector itself, a measurement in a second detector's position is required. The increase in statistics allows measuring a relevant number of η events exploiting its decays to two photons. This decay is the second most important contribution to photon production in the high energy atmospheric showers ($10 \div 20\,\%$). In the previous 13 TeV $p + p$ run LHCf collected only 500 events, identified as a peek centered at the η mass in the two photons invariant mass distribution. This statistics is clearly not enough to allow discriminating between the different models.

The last primary item is the measurement of neutral kaons. This measurement would be of considerable interest for the study of the production of the s-quark in hadronization. It represents also a relevant information for atmospheric neutrino production by charged kaons, due to the correlation between neutral and charged kaon prodction. According to simulations we expect approximately $5 \div 50$ events in the previous 13 TeV $p + p$ run, which have to be identified among the events with four photons hitting the two calorimeter towers ($K^0 \longrightarrow 2\,\pi^0 \longrightarrow 4\,\gamma$). The proposed run would allow collecting around few hundreds events corresponding to k_s^0 decays.

Assuming a pessimistic value of the achievable luminosity, $\mathscr{L}_{\text{min}} = 10^{29}\,\text{cm}^{-2}\text{s}^{-1}$, the collection of the proposed statistics requires slightly more than two days of data taking for two different positions of the detector. In case we consider a luminosity of $10^{30}\,\text{cm}^{-2}\text{s}^{-1}$, the nominal value requested by LHCf for this run, it would take approximately one day to complete the minimum physics program. The LHCf requests are summarized in table 5.

In case the common data taking with the ATLAS detector is approved, the requested DAQ time length would depend also on the common DAQ rate allowed by ATLAS. If the maximum LHCf DAQ rate (1.6 kHz) is accepted, the numbers in Table 5 remain the same, while in case the triggerIn case of horizontal beam crossing rate will be prescaled to a level of 600 Hz a factor 2 in the DAQ time has to be considered, as indicated in the table.

Run parameters for the LHCf minimum physics program with $p+p$ collisions at $\sqrt{s}$ =14 TeV ($L = 10^{30}\,\mathbf{cm^{-2}s^{-1}}$)	
Parameter	*Value*
Number of $p+p$ collisions per detector position	$\sim 3 \times 10^9$
Delivered integrated luminosity per detector position (nb^{-1})	~ 40
Recorded integrated luminosity per detector position (nb^{-1})	~ 20
Collision rate at IP1 (kHz)	80
Arm1/Arm2 acceptance	~ 0.12
Hit rate on Arm1/Arm2 (kHz)	~ 10
Typical DAQ rate (kHz, including dead time)	~ 1.0
Net operation time at max rate (h)	~ 24
Net operation time at 600 Hz with ATLAS (h)	~ 48
Total number of collected type I and II π^0 events	$\sim (2 \div 3) \times 10^6$
Total number of collected η events	$\sim 6 \times 10^4$

Table 5: Summary of run parameters proposed for $p+p$ collisions.

While the proposal of the LHCf collaboration is to allow the experiment to collect data at a luminosity $L = 10^{30}\,\mathrm{cm^{-2}s^{-1}}$, the possibility of situations that could prevent the achievement of this level during the initial phase of Run 3 has been considered. Table 6 shows the previous parameters evaluated in a pessimistic hypothetical scenario with a luminosity of the order of $10^{29}\,\mathrm{cm^{-2}s^{-1}}$. In this case the net operation time would be of the order of one week to complete the minimum physics program.

6.2 $p+O$ run at $\sqrt{s_{NN}} = 9.9\,\mathbf{TeV}$

The main purpose of a possible LHCf $p+O$ run is a precise measurement of forward particles in a clean configuration. In this section an estimation of the basic set of beam and run parameters for a hypothetical LHCf short run is presented. The same considerations done for the $p+p$ case for the evaluation of the beam crossing, pile-up of events and overlap of signals are valid also for the $p+O$ run. The basic request for LHCf for $p+O$ is a low luminosity run with a small number of colliding bunches plus some non colliding, for the measurement of photons, π^0s and neutrons. Table 7 summarizes the beam parameters proposed for a LHCf short run during $p+O$ collisions.

These values have already been presented to the LPC coordinators and will be discussed in the next months. The proposed luminosity is lower than the luminosity requested by the non-forward experiments, therefore the LHCf run could be seen as a special run.

According to the first evaluation a sensible improvement of the beam time could be achieved if LHCf could accept running with $\mu \sim 0.02 \div 0.03$, which is under evaluation.

According to the results of the 13 TeV run we estimate that a reasonable minimum number of registered events to produce relevant physics results for photons and neutrons

Run parameters for the LHCf minimum physics program with $p+p$ collisions at $\sqrt{s}$ =14 TeV ($L = 10^{29}\,\mathbf{cm^{-2}s^{-1}}$)	
Parameter	*Value*
Number of $p+p$ collisions per detector position	$\sim 3 \times 10^9$
Delivered integrated luminosity per detector position (nb^{-1})	~ 30
Recorded integrated luminosity per detector position (nb^{-1})	~ 20
Collision rate at IP1 (kHz)	8
Arm1/Arm2 acceptance	~ 0.12
Hit rate on Arm1/Arm2 (kHz)	~ 0.85
Typical DAQ rate (kHz, including dead time)	~ 0.6
Net operation time at max rate (days)	~ 7
Total number of collected type I and II π^0 events	$\sim (2 \div 3) \times 10^6$
Total number of collected η events	$\sim 6 \times 10^4$

Table 6: Summary of run parameters evaluated for $p+p$ collisions at low luminosity.

Beam parameters for the LHCf run with $p+O$ collisions at $\sqrt{s_{NN}}$ =9.9 TeV	
Parameter	*Value*
Bunches per beam	best: 43
Minimum bunch spacing (ns)	best: 2 (≥ 0.2)
Luminosity ($\mathrm{cm^{-2}s^{-1}}$)	$\lesssim 1 \times 10^{28}$
Inelastic cross-sections QCD/UPC (b)	0.5/0.005
μ (average n. of collisions per BC)	$\lesssim 0.01$
Beam crossing	vertical, downward
Beam crossing angle (μrad)	best: 290 (total)
β^* (m)	best: ~ 10 ($\gtrsim 1$)

Table 7: Summary of beam parameters proposed by for $p+O$ collisions.

is of the order of 2×10^7 for the nominal detector position. This corresponds to an integrated luminosity of about $0.7\,\mathrm{nb}^{-1}$ for a single detector position (nominal position). As for the $p+p$ case, LHCf requires a second measurement in a shifted detector position in such a way to extend the accessible phase space and cover the rapidity intervals not covered in the nominal position. Assuming a luminosity $\mathscr{L}_{\mathrm{min}} \simeq 10^{28}\,\mathrm{cm^{-2}s^{-1}}$, this statistics require slightly less than two days of data taking for two different positions of the detector. The LHCf requests are then summarized in Table 8.

Since the eventual light ion collision phase has not yet been approved and the relative possible running period has not yet been established, the LHCf collaboration is available to evaluate its participation to of this possible run with extreme flexibility, keeping in mind the primary constraints due to the radioprotection issues and to the interference with the ATLAS ZDC physics program.

Run parameters for the LHCf minimum physics program with $p+O$ collisions at $\sqrt{s_{NN}}$ =9.9 TeV	
Parameter	*Value*
Number of $p+O$ collisions (one detector position)	$\sim 3.5 \times 10^8$
Integrated luminosity (nb^{-1}, one detector position)	~ 0.7
Collision rate at IP1 (kHz)	~ 5
Arm1/Arm2 total acceptance	~ 0.08
Hit rate on Arm1/Arm2 (kHz)	~ 0.4
Max DAQ rate (kHz, including dead time)	~ 0.33
Net operation time at max rate (h)	~ 40
Total number of collected type I and II π^0 events	$\sim 4 \times 10^5$

Table 8: Summary table of proposed run parameters, event rates and expected data sets for a $p+O$ run.

6.3 $O+O$ run at $\sqrt{s_{NN}} = 7$ TeV

In case it is decided by the LHC to schedule an $O+O$ run instead of a $p+O$ run,the LHCf collaboration is interested to participate. Differently from $p+O$, because of the symmetry of the interaction, to minimize the impact on the ATLAS ZDC program, we propose to install only the Arm2 detector in the LSS1R zone, between IP1 and IP2. The detector must be operated at least 15 mm shifted upward from the interaction line. The cross section is approximately three times larger than for $p+O$, therefore a lower luminosity has to be required to maintain the pile-up at or below 1%. This can be done as long as the measure lasts longer, without worsening the quality of the results.

According to simulations performed as described in section 4.1.2, the cross section for UPC in $O+O$ at this energy is 0.31 b, much larger with respect to the $p+O$ case, relatively to the inelastic cross section (1.5 b). However, the LHCf acceptance of UPC events with the detector shifted upward by 15 mm is $\sim 1/5$ of the acceptance for QCD events, so the UPC contamination is expected to be of the order of 4%; this can be further decreased to 2% shifting upward the detector by 25 mm. With this low level of UPC background the subtraction of their contribution doesn't increase the systematic error of the measured photon and neutron spectra, as discussed in section 4.1.2. The main issue in the hypothesis of $O+O$ collisions is that, although the measurement is partly feasible, for LHCf it is not possible to access extreme pseudorapidities, thus loosing the possibility to study the most relevant region for the study of atmospheric cosmic-ray showers.

Table 9 summarizes the preliminary beam parameters proposed for a LHCf short run during $O+O$ collisions. For the minimum physics program in $O+O$ collisions, at the current stage we consider Table 8 as a starting point for the run parameter, with the exception of the duration of the measurements.

The LHCf run configuration in case of an $O+O$ run has still to be confirmed after

Beam parameters for the LHCf run with $O+O$ collisions at $\sqrt{s_{NN}}$ =9.9 TeV	
Parameter	*Value*
Bunches per beam	best: 43
Minimum bunch spacing (ns)	best: 2 (≥ 0.2)
Luminosity ($\mathrm{cm}^{-2}\mathrm{s}^{-1}$)	$\lesssim 3 \times 10^{27}$
Inelastic cross-sections QCD/UPC (b)	1.5/0.31
μ (average n. of collisions per BC)	$\lesssim 0.01$
Beam crossing	vertical, downward
Beam crossing angle (μrad)	best: 290 (total)
β^* (m)	best: ~ 10 ($\gtrsim 1$)

Table 9: Summary of preliminary beam parameters proposed by for O+O collisions.

a careful evaluation together with the ATLAS ZDC team, in such a way to minimize the interference between the two detectors and the different physics programs.

7 Common run with ATLAS central and forward detectors

Common LHCf-ATLAS data taking was already implemented successfully for the previous $p+Pb$ (2013), $p+p$ (2015) and $p+Pb$ (2016) runs. The main task for LHCf is the classification of the LHCf triggered events in different process-based categories, such as diffractive and non-diffractive events, as requested by the developers of the hadronic interaction models to improve their codes by tuning separately the different classes of events. This is possible by studying the correlation between the forward and the central particle productions, respectively measured by the LHCf and ATLAS detectors. The results of the first LHCf-ATLAS joint analysis to study the contribution of diffractive events in the forward photon production can be found in [10].

Currently there is no official agreement between the LHCf and ATLAS collaborations for a joint data taking for the eventual LHCf $p+p$ and light ion runs, but discussions have already been carried out recently between the management of the two collaborations, and both collaborations have confirmed their interest in such a possibility. The ATLAS collaboration supports a joint LHCf-ATLAS data taking for $p+p$ collisions as done for the previous runs. The possible inclusions of the ZDC and roman pots are under discussion. COncerning the eventual light ion run, the ATLAS ZDC group is interested in data taking for the ZDC own physics program. The effects of the interference between the ZDC and LHCf detectors and the impact on their physics programs are under evaluation. Different scenarios are considered, depending on the configuration of the run, which could include two consecutive phases for $p+O$ and $O+O$ collisions with or without interruption between them. An interruption would

result in a better flexibility and a modification of the installed detectors' setup could be considered, thus allowing for a minimization of the interference between the two detectors.

7.1 Implementation of the common data taking

To combine data from the two detectors, a joint LHCf - ATLAS trigger has been setup starting from the ion run between 2012 and 2013 [32], in the following way. The handshake at trigger level between the two experiments starts with the LHCf trigger system, identifying an event containing an high-energy particle candidate. This sets the LHCf data acquisition system to the 'enabled' mode. Within the LHCf fiducial volume the trigger system is 100% efficient for an incident photon with energy above 100 GeV [33] and about 40% efficient for an incident neutron with energy 400 GeV, reaching a 70% plateau for neutron energies above 2000 GeV [34]. This trigger signal is then sent to ATLAS, arriving at the ATLAS Level-1 Central Trigger Processor within $\simeq 1.5\,\mu$s after the collision. The LHCf trigger signal is then accepted as an ATLAS Level-1 trigger without further conditions, initiating the ATLAS event recording chain to readout the same event that generated the LHCf trigger. The ATLAS Level-1 accept (L1A) trigger signal is a single trigger pulse that is generated by the ATLAS Central Trigger Processor for every event passing the Level-1 trigger. The L1A pulses are counted in ATLAS for every event and stored as part of the event record. This L1A pulse was also sent back to LHCf, counted there, and similarly recorded in the LHCf event stream, thereby providing a single unique counter identifying every event that can be used to synchronize ATLAS and LHCf events offline. The ATLAS Level-2 trigger and Event Filter (EF) are higher level software trigger algorithms which allow a further processing of information and selection of events to save. ATLAS record the data triggered by LHCf triggers using the EF trigger EF_L1LHCF_NoAlg that does not make use of any further information at Level-2; hence it is purely based on the signals provided by LHCf.

In case of the $p + Pb$ run in 2013 the trigger rate at Level-1, approximately 700 Hz, was prescaled down to 10 Hz in order to fit into the allocated bandwidth. From the last $p + p$ run at 13 TeV the prescaling factor was removed and all the LHCf triggered events were accepted as ATLAS minimum bias events.

For the data taking proposed for Run3 the discussion of the common data acquisition rate is on-going with the ATLAS relevant persons.

7.2 Common operation with ATLAS ZDC and Roman Pots

A DAQ operation in common with ATLAS ZDC and Roman Pots, that has not been well performed in the last LHCf data taking period, will allow a significant improvement in the neutron energy resolution, hence opening new physics channels, as described in section 3.2. However, we still need some discussions and some common studies with

the ATLAS members to finally agree and realize this joint operation plan. The Roman Pots performance strongly depends on the beam optics and the LHCf normal operation conditions, shown in table 4, are not the optimal one for them. Studies with different possible beam optics are on-going to maximize the physics potential of the LHCf-ATLAS Roman Pots common run.

References

[1] O. Adriani *et al.*, "Measurements of longitudinal and transverse momentum distributions for neutral pions in the forward-rapidity region with the LHCf detector," *Phys. Rev.*, vol. D94, no. 3, p. 032007, 2016.

[2] K.-H. Kampert and M. Unger, "Measurements of the Cosmic Ray Composition with Air Shower Experiments," *Astropart. Phys.*, vol. 35, pp. 660–678, 2012.

[3] K. Akiba *et al.*, "LHC Forward Physics," *J. Phys.*, vol. G43, p. 110201, 2016.

[4] O. Adriani *et al.*, "Measurement of zero degree inclusive photon energy spectra for $\sqrt{s} = 900$ GeV proton-proton collisions at LHC," *Phys. Lett.*, vol. B715, pp. 298–303, 2012.

[5] O. Adriani *et al.*, "Measurement of zero degree single photon energy spectra for $\sqrt{s} = 7$ TeV proton-proton collisions at LHC," *Phys. Lett.*, vol. B703, pp. 128–134, 2011.

[6] O. Adriani *et al.*, "Measurement of very forward neutron energy spectra for 7 TeV protonproton collisions at the Large Hadron Collider," *Phys. Lett.*, vol. B750, pp. 360–366, 2015.

[7] O. Adriani *et al.*, "Measurement of forward neutral pion transverse momentum spectra for $\sqrt{s} = 7$TeV proton-proton collisions at LHC," *Phys. Rev.*, vol. D86, p. 092001, 2012.

[8] O. Adriani *et al.*, "Transverse-momentum distribution and nuclear modification factor for neutral pions in the forward-rapidity region in proton-lead collisions at $\sqrt{s_{NN}} = 5.02$ TeV," *Phys. Rev.*, vol. C89, no. 6, p. 065209, 2014.

[9] O. Adriani *et al.*, "Measurement of forward photon production cross-section in proton-proton collisions at $\sqrt{s} = 13$ TeV with the LHCf detector," *Phys. Lett.*, vol. B780, pp. 233–239, 2018.

[10] "Measurement of contributions of diffractive processes to forward photon spectra in pp collisions at $\sqrt{s} = 13$ tev," Tech. Rep. ATLAS-CONF-2017-075, CERN, Geneva, Nov 2017.

[11] O. Adriani *et al.*, "Measurement of inclusive forward neutron production cross section in proton-proton collisions at $\sqrt{s} = 13$ TeV with the LHCf Arm2 detector," *JHEP*, vol. 11, p. 073, 2018.

[12] T. Pierog, "Synergies with astroparticles, nuclear and neutrino physics." `https://indico.cern.ch/event/808335/contributions/3367983/attachments/1842407/3025564/synergy_astroparticles_pierog.pdf`.

Granada Open Symposium - Update of the European Strategy for Particle Physics, 2019.

[13] Z. Citron *et al.*, "Future physics opportunities for high-density QCD at the LHC with heavy-ion and proton beams," Tech. Rep. arXiv:1812.06772, CERN, Geneva, 2018.

[14] S. Ostapchenko, "Monte Carlo treatment of hadronic interactions in enhanced Pomeron scheme: I. QGSJET-II model," *Phys. Rev.*, vol. D83, p. 014018, 2011.

[15] F. W. Bopp, J. Ranft, R. Engel, and S. Roesler, "Antiparticle to Particle Production Ratios in Hadron-Hadron and d-Au Collisions in the DPMJET-III Monte Carlo," *Phys. Rev.*, vol. C77, p. 014904, 2008.

[16] S. Ostapchenko, M. Bleicher, T. Pierog, and K. Werner, "Constraining high energy interaction mechanisms by studying forward hadron production at the LHC," *Phys. Rev.*, vol. D94, no. 11, p. 114026, 2016.

[17] V. A. Khoze, A. D. Martin, and M. G. Ryskin, "Total $\pi^+ p$ cross section extracted from the leading neutron spectra at the LHC," *Phys. Rev.*, vol. D96, no. 3, p. 034018, 2017.

[18] J. J. Chwastowski, S. Czekierda, R. Staszewski, and M. Trzebiński, "Diffractive bremsstrahlung at high-β ˆ\star LHC. Case study," *European Physical Journal C*, vol. 77, p. 216, Apr. 2017.

[19] S. Klein and J. Nystrand, "Exclusive vector meson production in relativistic heavy ion collisions," *Phys. Rev.*, vol. C60, p. 014903, 1999.

[20] "STARLIGHT webpage." `https://starlight.hepforge.org`.

[21] A. Mucke, R. Engel, J. P. Rachen, R. J. Protheroe, and T. Stanev, "SOPHIA: Monte Carlo simulations of photohadronic processes in astrophysics," *Comput. Phys. Commun.*, vol. 124, pp. 290–314, 2000.

[22] "SOPHIA webpage." `https://www.uibk.ac.at/projects/he-cosmic-sources/tools/sophia/index.html.en`.

[23] "DPMJET webpage." `http://sroesler.web.cern.ch/sroesler/dpmjet3.html`.

[24] P. S. T. Sjstand, S. Mrenna, "Pythia 6.4 physics and manual," *JHEP*, vol. 05, p. 026, 2006.

[25] "PYTHIA 6.4 webpage." `http://pythia6.hepforge.org`.

[26] O. Adriani *et al.*, "Transverse-momentum distribution and nuclear modification factor for neutral pions in the forward-rapidity region in proton-lead collisions at $\sqrt{s_{NN}} = 5.02$ TeV," *Phys. Rev.*, vol. C89, no. 6, p. 065209, 2014.

[27] O. Adriani *et al.*, *LHCf experiment: Technical Design Report*. CERN-LHCC-2006-004, Geneva: CERN, 2006.

[28] O. Adriani *et al.*, "The LHCf detector at the CERN Large Hadron Collider," *JINST*, vol. 3, p. S08006, 2008.

[29] O. Adriani *et al.*, "The construction and testing of the silicon position sensitive modules for the LHCf experiment at CERN," *JINST*, vol. 5, p. P01012, 2010.

[30] Y. Itow *et al.*, "Recent results from the LHCf and RHICf experiments," *EPJ Web Conf.*, vol. 208, p. 05004, 2019.

[31] "Talk by N. Karastathis at the EVIAN 2019."

[32] "LHCf+ATLAS common trigger setup, howpublished = `https://edms.cern.ch/document/930829/1`."

[33] A. Tiberio, *Study of the very forward electromagnetic component produced in proton-proton collisions at $\sqrt{s}$ = 13 TeV with the LHCf experiment*. CERN-THESIS-2017-045.

[34] E. Berti, *Measurement of the energy spectra relative to neutrons produced at very small angle in* $\sqrt{\mathrm{s}} = 13$ TeV *proton-proton collisions using the LHCf Arm2 detector*. CERN-THESIS-2017-035.